

# Improving RF-DNA Fingerprinting Performance In An Indoor Multipath Environment Using Semi-Supervised Learning

Mohamed K. M. Fadul, Donald R. Reising<sup>†</sup>, Lakmali P. Weerasena, T. Daniel Loveless, Mina Sartipi, Joshua H. Tyler\*  
The University of Tennessee at Chattanooga  
Chattanooga, TN 37403 USA

Email: {mohammed-fadul, donald-reising<sup>†</sup>, lakmali-weerasena, daniel-loveless, mina-sartipi}@utc.edu, ygml11@mocs.utc.edu\*

**Abstract**—The number of Internet of Things (IoT) deployments is expected to reach 75.4 billion by 2025. Roughly 70% of all IoT devices employ weak or no encryption; thus, putting them and their connected infrastructure at risk of attack by devices that are wrongly authenticated or not authenticated at all. A physical layer-based security approach—known as Specific Emitter Identification (SEI)—has been proposed and is being pursued as a viable IoT security mechanism. SEI is advantageous because it is a passive technique that exploits inherent and distinct features that are unintentionally imparted upon the signal during its formation and transmission within and by the IoT device’s Radio Frequency (RF) front-end. SEI’s passive exploitation of unintentional signal features removes any need to modify the IoT device, which makes it ideal for existing and future IoT deployments. Despite the amount of SEI research conducted there remains challenges that must be addressed to make SEI a viable IoT security approach. One of these challenges is the extraction of SEI features from signals collected under multipath fading conditions. Multipath corrupts the inherent SEI exploited features that are used to discriminate one IoT device from another; thus, degrading authentication performance and increasing the chance of attack. This work presents two semi-supervised Deep Learning (DL) equalization approaches and compares their performance with the current state of the art. The two approaches are the Conditional Generative Adversarial Network (CGAN) and Joint Convolutional Auto-Encoder and Convolutional Neural Network (JCAECNN). Both approaches learn the channel distribution to enable multipath correction while simultaneously preserving the SEI exploited signal features. CGAN and JCAECNN performance is assessed using a Rayleigh fading channel under degrading SNR, up to thirty-two IoT devices, as well as two publicly available signal sets. The JCAECNN improves SEI performance by 10% beyond that of the current state of the art.

**Index Terms**—Deep Learning, Specific Emitter Identification (SEI), Internet of Things (IoT), Security

## I. INTRODUCTION

It is estimated that the number of operational Internet of Things (IoT) devices will reach 75.4 billion by 2025 [1]. Disturbingly, roughly seventy-percent of IoT devices employ weak or no encryption at all due to limited onboard resources (e.g., memory, computation, etc.), manufacturing costs that prohibit adoption, or difficulties associated with key management and implementation at scale [2]–[4]. The lack of or

limited encryption creates a security vulnerability that leaves individual IoT devices and corresponding infrastructure open to exploitation by nefarious actors [5]–[12]. Based upon this observation and attacks there is a critical need for an effective IoT security solution.

IoT deployments conform to the Open Systems Interconnection (OSI) model, which states that the Physical (PHY) layer is responsible for completing point-to-point bit stream communication and is considered the lowest and first layer [13]. By design, traditional security techniques are implemented at higher OSI layers (e.g., Data Link or Network); thus, they do not consider the PHY layer despite the fact that attackers must traverse it to conduct their attacks [14]. Specific Emitter Identification (SEI) has been proposed as a PHY layer IoT security solution [15]–[17]. SEI has been shown capable of achieving serial number discrimination by exploiting immutable, unintentional coloration that is imparted upon a signal during its formation and transmission. The coloration’s source is attributed to the tolerated, manufacturing variation(s) present within the individual components, sub-systems, and systems that comprise an emitter’s Radio Frequency (RF) front-end [14], [18]–[38]. SEI is advantageous because it provides a passive authentication mechanism that does not require modification of the end device (i.e., the coloration is generated as part of normal operations), which makes it ideally suited to IoT applications since there is no additional resource demands placed on the device being identified. However, since its inception—almost thirty years ago—very little attention has been paid to the performance of SEI within contentious operating conditions such as multipath. SEI’s viability—as an IoT security solution—rests on it remaining effective even under degrading operating conditions.

RF-Distinct Native Attributes (RF-DNA) fingerprinting is an SEI implementation that extracts exploitable features from portions of the transmitted signal corresponding to fixed, known symbol sequences such as the IEEE 802.11a Wireless-Fidelity (Wi-Fi) preamble. Prior RF-DNA fingerprinting research uses supervised and unsupervised learning algorithms that rely on expert knowledge and handcrafted features to facilitate IoT device discrimination [14], [17], [21], [23]–[26], [34]–[41]. These algorithms may results in sub-optimal models that limit RF-DNA fingerprinting performance, especially under

<sup>†</sup> – Corresponding author.

This work supported in part by the University of Chattanooga (UC) Foundation, Inc.

TABLE I  
NOTATIONS.

$N_D$	Number of emitters used in this work	$N_B$	Number of collected signals per emitter	$A, B$	I.I.D random variables
$\sigma^2$	Variance	$L$	Length of Rayleigh fading channel	$T_r$	Root-Mean-Squared of the delay spread
$T_s$	Sampling period	$\alpha_k$	Coefficient of the $k^{th}$ Rayleigh fading path	$\tau_k$	Delay of the $k^{th}$ Rayleigh fading path
$x(t)$	Collected IEEE 802.11a signal	$r(t)$	Received signal with multipath	$n(t)$	Complex, white Gaussian noise
$h(t)$	TDL channel impulse response	$\hat{x}(m)$	Estimate of the transmitted signal $x(m)$	$\gamma$	Signal-to-Noise ratio (SNR)
$I_A$	Identity matrix with matching dimensions to $A$	$\beta$	NN activation function	$W$	Weights of the convolutional kernel
$\mathcal{F}$	Set of RF-DNA fingerprints with class labels	$b$	NN bias	$\theta$	Trainable parameters of the NN
$J(\theta)$	Loss function of the NN	$D(x)$	Discriminator's output for input $x$	$G(z)$	Generator's output for input $z$
$P_d(x)$	Distribution of training data $x$	$P_z(z)$	Prior probability of $G$ 's input $z$	$r_{\mathcal{R}}(n)$	Received signal In-phase component
$r_{\mathcal{I}}(n)$	Received signal Quadrature component	$\rho_r$	Magnitude of the received signal	$\theta_r$	Phase angle of the received signal
$N_R$	Number of training signals per emitter	$N_T$	Number of testing signals per emitter	$\tilde{x}[n]$	AWGN channel output for input $x[n]$
$y$	Actual Label corresponding to the transmitted signal $x[n]$	$\tilde{X}_e$	IQ+NL labeled representation of $\tilde{x}[n]$	$\mathbf{R}_e$	IQ+NL labeled representation of $r[n]$
$\hat{X}_e$	$G$ 's output for input $\mathbf{R}_e$	$\tilde{y}_c$	Estimated label by the JCAECNN classifier	$C_k$	Delayed and scaled version of the transmitted signal $x[n]$
$N_z$	Number of noise realizations	$z$	Input to the CGAN generator, $G$		

degraded operating conditions such as time-varying or lower Signal-to-Noise Ratio (SNR) channels. Over the past five years the SEI research community has pursued Deep Learning (DL) due to its successful application in spectrum management [42], [43], modulation and emitter identification [44]–[46], system design [44], [47]–[50], as well as its ability to thrive under increasing amounts of information while removing the need for handcrafted features [35], [46], [51]–[85]. Based upon the success of these published DL works, our work—presented herein—shows that DL can provide an effective RF-DNA fingerprinting process capable of facilitating serial number discrimination of IoT devices under degraded operating conditions. Specifically, we show that up to thirty-two IoT devices—that only differ in serial number—can be successfully discriminated from one another within an indoor multipath channel environment.

The remainder of this paper is organized as follows. Sect. II summarizes current publications that are most pertinent to our work as well as providing a more detailed description of our work's contributions. Sect. III provides descriptions of the; signal of interest, signal collection and detection processes, multipath channel modeling, Nelder-Mead (N-M) channel estimator and Minimum Mean Square Error (MMSE) equalizer, as well as the deep learning architectures used herein. The methodology for the developed DL-driven RF-DNA fingerprinting approach for indoor multipath environments is described in Sect. IV. The results are presented in Sect. V and the article concluded in Sect. VI.

## II. RELATED WORK AND CONTRIBUTION

DL-based SEI has been shown to provide an optimal end-to-end solution that results in superior performance, however

most of the published works do not conduct SEI using RF signals that have undergone time-varying fading. In fact, only a small subset of DL-based SEI works have assessed its performance under multipath conditions and most can be categorized as using a channel that is: (i) static (i.e., the channel coefficients or characteristics never change) [35], or (ii) time-varying, but the environments specific characteristics (e.g., number of reflectors, line-of-sight present or not, type of fading, etc.) are unknown, unstated, or not disclosed by the authors [35], [46], [53], [62], [63], [74], [76], [81]. Regardless, most DL-based SEI efforts assume the selected, modified, or developed algorithm can learn discriminatory features directly from the received signals; thus, eliminating the need for channel estimation and correction prior to RF signal classification. The fact is that the time-varying nature of multipath fading channels impedes or significantly hinders the DL algorithms' ability to learn discriminating signal features that are invariant to multipath fading.

The work in [41] is the exception to this trend in that the authors: (i) adopt the IEEE 802.11a Wi-Fi indoor, channel model and state the specific values used to configure it [86] as well as (ii) perform traditional (i.e., not DL-based) multipath channel estimation and correction prior to performing SEI using a Convolutional Auto-Encoder (CAE) initialized Convolutional Neural Network (CNN). The authors' use of traditional estimation and correction approaches results in sub-optimal SEI performance due to errors in the estimated channel coefficients and a dependence on knowing the channels' statistics. Lastly, the authors assess their CAE-CNN SEI approach using only four emitters, which does not reflect typical IoT deployments consisting of tens to hundreds of devices.

Our work—presented in detail in the remainder of this paper—advances DL-based SEI’s current state of the art through the following contributions:

- 1) Combining label embedding with a Conditional Generative Adversarial Network (CGAN) to efficiently learn each emitter’s conditional feature distribution.
- 2) Augmenting discriminatory feature learning through the use of the rectangular and polar signal representation [87].
- 3) Introduces and assesses two semi-supervised learning equalization approaches that facilitate superior CNN-based SEI under Rayleigh fading and degrading SNR conditions.
- 4) Introduces and assesses a scalable, semi-supervised learning architecture that jointly develops CAE-based generative models and a CNN-based discriminative model to correct for Rayleigh fading while preserving SEI discriminative features. This joint architecture—designated herein as JCAECNN—decomposes the multipath signal into individual scaled and delayed versions of the original transmitted signal prior to CNN classification.
- 5) Improving our JCAECNN’s SEI performance through the use of exponentially decaying loss function weights.
- 6) SEI performance assessment of the CGAN and JCAECNN architectures as four, eight, sixteen, or thirty-two emitters communicate over a Rayleigh fading channel.
- 7) JCAECNN SEI performance assessment using the public signal sets generated by the authors of [88], [89]. These results serve as a benchmark to permit comparative assessment with current and future publications.
- 8) Directly compares the CGAN and JCAECNN architectures’ SEI performance with our prior work in [38], [41].

These contributions result in an average percent correct classification performance of 94.35% or better for SNR values of 9 dB or higher, Rayleigh fading channels comprised of five reflections/paths and an IoT deployment consisting of sixteen devices.

### III. BACKGROUND

#### A. Signal of Interest

This work makes use of IoT emitters that communicate using the IEEE 802.11a Wi-Fi protocol. The reasons for choosing the IEEE 802.11a protocol for the signal sub-layer are as follows: (i) 802.11a is based on Orthogonal Frequency Division Multiplexing (OFDM) signal, which is used in multiple wireless communication standards such as 802.11ac, 802.11ad, 802.11ax, Long Term Evolution (LTE), and Worldwide Interoperability for Microwave Access (WiMAX) [90], (ii) multiple research efforts within the SEI community have demonstrated success using 802.11a signals [18], [21], [24], [27], [33], [34], [36]–[39], [46], [56], [85], [87], [91], (iii) availability of the same data set used in our previous publications [36]–[38], [41], [85], [87] to facilitate comparative assessments, and (iv) 802.11a Wi-Fi has been adopted as an IoT communications protocol [92]. Consistent with our prior publications, this work performs SEI by extracting RF-DNA fingerprints from the IEEE 802.11a Wi-Fi preamble, which comprises the first 16  $\mu$ s

of every transmission [36]–[38], [41]. Use of the 802.11a preamble is ideal, because it is the portion of the signal used by the receiver to perform channel equalization. An 802.11a preamble consists of ten—designated  $t_1$  through  $t_{10}$ —Short Training Symbols (STS), a Guard Interval (GI), and two Long Training Symbols (LTS) that are designated  $T_1$  and  $T_2$  in Fig. 1 [93].

#### B. Signal Collection & Detection

The primary data set used in this work is comprised of 802.11a Wi-Fi signals transmitted by  $N_D = 4$  Cisco AIR-CB21G-A-K9 Wi-Fi emitters and collected using an Agilent E3238S-based spectrum analyzer. The spectrum analyzer can sample signals at rates up to 95 mega-samples per second (Msps), has an operating range from 20 MHz to 6 GHz, an RF bandwidth of 36 MHz, and a 12-bit analog-to-digital converter [94]. Upon collection, a total of  $N_B = 2,000$  signals are selected for each of the  $N_D = 4$  emitters using amplitude-based variance trajectory detection [23]. After that, each signal is filtered using a fourth order low-pass Butterworth filter with a cutoff frequency of 7.7 MHz. Following filtering, the signals are post-processed by correcting for carrier frequency offset and downsampled to 20 MHz [39].

#### C. Multipath Channel Modeling

Multipath is a major concern for communications systems operating in indoor environments. It degrades system performance by limiting the receiver’s ability to correctly recover the transmitted message. This degradation is due to multiple copies of the transmitted signal—associated with different delays and attenuation values—destructively interfere with one another at the receiver’s antenna(s). These copies are reflections of the transmitted signal off of objects located throughout the propagation environment [86]. The combination of these reflected copies—at the receiver—randomly shifts the carrier frequency between the transmitter and receiver as well as changes the signal strength over short time intervals [86]. For the work presented in this article, the indoor, multipath channels are modeled using a Rayleigh distribution for two reasons: (i) this distribution is used to assess Wi-Fi modulation performance by the IEEE 802.11 working group [86], and (ii) prior SEI publications have used or assessed system performance using the same distribution [36]–[38], [41], [53], [74], [76], [81].

In multipath fading, a single reflection (a.k.a., path) is quantified using coefficient and a corresponding time delay known as a delay spread [86]. For the case of Rayleigh fading,

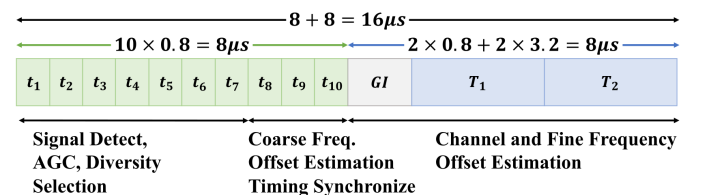


Fig. 1. Structure of the 16  $\mu$ s duration preamble that is present at the start of every IEEE 802.11a Wi-Fi frame [93].

a Tap Delay Line (TDL) is used to mathematically describe the channel. In a TDL, each ‘‘tap’’ represents a single coefficient and delay. For each path  $k$ , the coefficient is represented using a circularly symmetric complex Gaussian random variable,

$$\alpha_k = A + jB, \quad (1)$$

where  $k = 1, \dots, L$  for a total number of  $L$  paths comprising the channel, and  $\sigma^2$  is the variance of the zero mean independent and identically distributed Gaussian random variables  $A$  and  $B$  [86]. If the delay spread’s Root-Mean-Squared (RMS) is  $T_r$  and the sampling period is  $T_s$ , then the variance can be defined as,

$$\sigma^2 = \frac{\sigma_k^2}{2} = \frac{1}{2} \left\{ \left[ 1 - \exp\left(\frac{-T_s}{T_r}\right) \right] \exp\left(\frac{-kT_s}{T_r}\right) \right\}. \quad (2)$$

Finally, the TDL for a multipath environment consisting of  $L$  total reflecting paths is,

$$h(t) = \sum_{k=1}^L \alpha_k \delta(t - \tau_k T_s), \quad (3)$$

where  $\alpha_k$  and  $\tau_k$  are the coefficient and delay spread associated with the  $k^{\text{th}}$  path [86], [95]. A received signal with multipath is generated by,

$$r(t) = x(t) * h(t) + n(t), \quad (4)$$

where  $x(t)$  is a collected 802.11a Wi-Fi signal,  $h(t)$  is the TDL from (3),  $n(t)$  is complex, white Gaussian noise, and  $*$  denotes the convolution operation. The noise  $n(t)$  is filtered, scaled, and added to the result of  $x(t) * h(t)$  to generate multipath signals with SNR values from 9 dB to 30 dB in increments of 3 dB between consecutive values.

#### D. Traditional Channel Estimations & Equalization

This section explains the Nelder-Mead (N-M) estimator and MMSE equalizer, which are used here to facilitate comparative assessment between our results in Sect. V and those presented in our published work [41].

1) *Nelder-Mead Channel Estimator*: The N-M estimator is constructed using the N-M simplex algorithm, which minimizes unconstrained optimization problems using a direct search approach [96]. The N-M simplex algorithm iteratively determines a  $d$ -variable, non-linear function’s minimum solution using only function values and four defined operations. The N-M simplex algorithm is computationally efficient, because it does not require computation of the function derivatives [97]. At the start of iteration  $j$ , a  $d+1$  vertices simplex is defined, one or more of four operations—reflection, expansion, contraction, and shrinkage—are performed to calculate one or more new points, and the function’s values calculated using the new point(s). If the calculated function values at vertices given by  $x_1$  through  $x_{d+1}$  satisfy certain conditions, then the new point(s) replace the worst point(s) in the simplex that is denoted as  $x_{d+1}$  [96], [97]. If none of the first three operations’ conditions are satisfied, then a new set of points— $v_2$  through

$v_{d+1}$ —are calculated using the shrinkage operation using the following formula [97],

$$v_i = x_i + \varphi(x_i - x_1), \quad (5)$$

where  $1 < i \leq d+1$ , and the new simplex for the next iteration is  $(x_1, v_2, \dots, v_{d+1})$  [97]. The N-M simplex algorithm stops when the calculated function value—at iteration  $j$ —satisfies a certain termination condition or conditions. The termination conditions used in estimating the Rayleigh fading channel’s coefficients are the same as those used in [36]–[38], which are given by the following formulas,

$$\frac{1}{d} \sum_{i=1}^{d+1} [f(x_i) - \bar{f}]^2 < \epsilon_1, \quad (6)$$

$$\frac{1}{d} \sum_{i=1}^d \|x_i^j - x_i^{j+1}\|^2 < \epsilon_2, \quad (7)$$

where  $\bar{f}$  is the average of the function values  $f(x_i)$ ,  $\|\bullet\|$  is the  $l_2$ -norm, and  $\epsilon_1$  and  $\epsilon_2$  are tolerances based on the function values  $f(x_i)$  and points  $x_i$  respectively. Both conditions are checked at the end of each iteration. The function to be minimized is,

$$f(h) = \sum_{m \in T} \left| r(m) - \sum_{k=1}^L x(m - \tau_k) \alpha_k \right|^2. \quad (8)$$

The function  $f(h)$  can be described as a square error function between the received signal and the weighted and delayed copies of the transmitted signal  $x(m)$  [37]. Equation (8) is minimized in two parts because  $r(m)$  and  $x(m)$  are complex-valued while the N-M simplex algorithm solves real-valued functions [96], [97]. The two parts are created by separating the complex-valued signals into their real and imaginary components; thus, resulting in two real-valued, square error functions [36]. The N-M simplex algorithm is applied to each function separately to calculate the coefficient values  $\alpha_k$  and the estimation error reduced by using the average of the estimates from the two square error functions as the final coefficient estimates [36]. As in [36]–[38], [41], five ‘‘candidate’’ preambles are randomly selected from each of  $N_D = 4$  IEEE 802.11a emitters’ set of signals to represent the transmitted signal  $x(m)$ . Using the N-M simplex algorithm to solve equation (8)—for each candidate preambles—results in a total of  $N_C = 20$  channel impulse response estimates. The residual power formula is given as [25],

$$\hat{h}(m) = \arg \min_c \left\{ \sum_m |r(m) - \hat{h}_c(m) * x_c(m)|^2 \right\}, \quad (9)$$

and used to select the best channel estimate. Where  $\hat{h}_c(m)$  is the estimated channel impulse response corresponding to the candidate preamble  $x_c(m)$ , and  $1 \leq c \leq N_C$  [37].

2) *MMSE Channel Equalizer*: After estimating the channel impulse response, using the N-M estimator, the MMSE algorithm is used to correct for the multipath channel effects. The MMSE equalizer attempts to reconstruct the transmitted signal from the received signal by integrating channel statistics—such as the noise power—along with the estimated multipath channel coefficients [36]. The MMSE’s Inclusion of the channel statistics in the equalization process makes it a more robust approach under degrading SNR conditions. The MMSE equalizer aims to reduce the the squared error between the estimated  $\hat{x}(m)$  and original  $x(m)$  transmitted signals as follows,

$$\hat{x}(m) = \arg \min_{\hat{x}(m)} E [(x(m) - \hat{x}(m))^2]. \quad (10)$$

If the noise power or channel SNR is known, then the MMSE estimates the transmitted signal by solving,

$$\hat{\mathbf{x}}_M = \mathbf{A}^H (\mathbf{A}\mathbf{A}^H + \gamma^{-1}\mathbf{I}_A)^{-1} r \quad (11)$$

where  $\mathbf{A}$  is a 2D matrix representing the estimated channel impulse response,  $\gamma$  is the SNR, and  $\mathbf{I}_A$  is an identity matrix with matching dimensions to  $\mathbf{A}$  [98].

### E. Deep Learning Architectures

This section provides brief explanations of each DL architecture and algorithm used to generated the results in Sect. V.

1) *Convolutional Neural Network*: Convolutional Neural Networks (CNNs) are supervised learning Multi-Layer Perceptron (MLP)-based Neural Networks (NNs) designed to process multi-dimensional data in a grid architecture. It can be used to process a one-dimensional vector such as time-interval data, two-dimensional and three-dimensional grids of pixels such as images [99]. CNNs learn parameters  $\theta$  using the back-propagation algorithm to estimate a mapping function of a discriminative model by minimizing a loss function. The loss function computes the error between the model’s prediction and the ground truth.

The CNN network is comprised of a MLP prepended with convolutional and pooling layers. Convolutional layers consist of multiple neurons in a grid structure where each neuron corresponds within an element-wise multiplication of a multi-dimensional kernel (a.k.a., filter) and a region in the input that is the same size as the kernel. The kernel’s elements are called weights and they are shared between all neurons [100]. In a CNN, convolutional layer(s) are used to detect and extract features from multiple regions of the input data to generate feature maps. Each neuron applies an activation function within the convolutional layer to non-linearly transform the feature map’s corresponding element [56], [100]. Pooling layers normally follow convolutional layers to reduce the dimensionality of the activated feature map by computing a statistic summary such as a maximum, minimum, and average of nearby outputs [99]. Max pooling is the most common pooling layer used in CNN networks. In this work, Max Pooling is adopted to extract the maximum-value features within rectangular frames of the activated feature maps. After

one or more convolutional and pooling layer stages, fully connected layers (a.k.a., dense layers) are used to detect high level features and pass them onto the output layer [46]. The purpose of the output layer is to predict the label to which the extracted features belong. In this work CNNs are adopted to implement RF-DNA fingerprint classification using IEEE 802.11a Wi-Fi preambles that transverse a Rayleigh fading channel under degrading SNR.

2) *Auto-Encoder*: An Auto-Encoder (AE) is an MLP-based NN that attempts to regenerate a multi-dimensional input at the output with as little error as possible [101], [102]. An AE is an unsupervised learning-based architecture used to learn the distribution and an efficient representation of the input data. Logically, an AE consists of two main parts: the encoder and decoder. Generally, the encoder attempts to estimate a mapping function that outputs an intermediate hidden representation  $\mathbf{h} = f(\mathbf{x})$ . The decoder aims to reconstruct the input from the hidden representation by applying another mapping function  $g(\mathbf{h})$  so the final output is  $\mathbf{r} = g(\mathbf{h}(\mathbf{x}))$  is as close as possible to the input  $\mathbf{x}$  [99]. During training, the AE’s loss function penalizes the decoder’s output for being different from  $\mathbf{x}$ . This work uses the Mean Square Error (MSE) as the loss function for all AEs. When the encoder is comprised of convolutional and pooling layers, the AE is designated a Convolutional AE (CAE). If the multi-dimensional data (a.k.a., tensor) at the CAE input is  $\mathbf{x}$ , then the hidden representation corresponding to the  $i^{\text{th}}$  tensor is given by,

$$h_i = \beta(x_i * W + b), \quad (12)$$

where  $W$  are the elements (a.k.a., weights) of the convolutional kernel,  $b$  is the bias,  $*$  denotes the convolution operation, and  $\beta$  is the activation function [102]. The decoder’s output  $r_i$  for  $h_i$  is given by,

$$r_i = \beta(h_i * \tilde{W} + \tilde{b}), \quad (13)$$

where  $\tilde{W}$  are the deconvolutional kernel weights, and  $\tilde{b}$  is the decoder’s bias [102]. During training, the CAE parameters—including  $W$ ,  $\tilde{W}$ ,  $b$ , and  $\tilde{b}$ —are adjusted using backpropagation to minimize the loss function given by,

$$J(\theta) = \sum_{i=1}^m (x_i - r_i)^2, \quad (14)$$

where  $m$  is the number of training samples.

3) *Generative Adversarial Networks*: A Generative Adversarial Network (GAN) is a DL-based architecture that aims to estimate a generative model by simultaneously training two deep network models using adversarial training. GANs can be used to estimate generative models for multiple applications including: image editing, style transfer, and image synthesis [103]. A GAN is comprised of two models referred to as the Generator,  $G$ , and the Discriminator,  $D$ . The  $G$  is a generative network that learns the training data distribution so it can generate new samples with the same distribution. The  $D$  is a discriminative network tasked with determining whether an input sample belongs to the training data set or was

generated by the  $G$ . GAN training can be viewed as a minimax two-player game in which the  $G$  attempts to learn the training data distribution and estimate a mapping function capable of generating new samples that increase the  $D$ 's probability of making the wrong decision, while  $D$  tries to maximize its probability of making the right decision (i.e., differentiating a training sample from a generated one) [99], [104]. The training results in a unique solution when the  $D$ 's output is uniformly distributed with a probability of one-half everywhere.

When MLP networks are used for both the  $G$  and  $D$  networks, backpropagation can be used to train the entire system where the NN representing the  $G$  recovers the data distribution without access to the training data and  $D$  maximizes the probability of making the right binary decision [103], [104]. If the prior probability of  $G$  input  $\mathbf{z}$  is  $P_{\mathbf{z}}(z)$ , then the generator mapping function can be given by  $G(\mathbf{z}; \theta_g)$  where  $\theta_g$  is the MLP parameters of  $G$ . The  $D$  function is given by  $D(\mathbf{x}; \theta_d)$  for input  $\mathbf{x}$  and a single output  $D(\mathbf{x})$ , which represents the probability that  $\mathbf{x}$  came from the training data and not the  $G$  [104]. During GAN training, the  $G$  network intends to learn the distribution  $P_g$  over the training data  $\mathbf{X}$  by simultaneously maximizing the correct decision probability  $D(\mathbf{x})$  and minimizing the term  $(1 - D(G(\mathbf{z})))$  corresponding to the  $G$  network [104]. The GAN minimax optimization problem can be described by the following objective function,

$$\min_G \max_D V(D, G) = E_{x \sim P_d(x)} \{\log[D(x)]\} + E_{z \sim P_z(z)} \{\log[1 - D(G(z))]\}, \quad (15)$$

where  $E$  is the expected value. The optimum point is reached when the  $G$  perfectly recovers the training data distribution (i.e.  $P_g = P_{data}$ ) [99], [104].

#### IV. METHODOLOGY

This section describes a nontraditional, pre-processing approach that uses semi-supervised DL to correct for multipath channel effects while simultaneously preserving the SEI exploited RF-DNA fingerprints. In fact, two semi-supervised learning-based channel equalization approaches are investigated. The first approach leverages the GAN architecture's adversarial relationship to train the  $G$  such that it learns the distribution of the multipath channel effects as well as the signals' RF-DNA fingerprints to create a mapping function capable of estimating and correcting the multipath channel effects. The second approach jointly trains a CAE and CNN architecture—designated herein as JCAECNN—that corrects the multipath channel effects while simultaneously improving the system's ability to extract more discriminative SEI features.

A Rayleigh fading channel comprised of  $L$  paths is applied to each collected IQ preamble to simulate a multipath environment. Each semi-supervised learning approach is used to equalize the resulting multipath preamble set with the goal of maximizing SEI performance. Motivated by the results in [87], semi-supervised learning is conducted using the raw

IQ preamble samples as well as their Natural Logarithm (NL) representation. The NL of the raw IQ samples is given by,

$$\begin{aligned} \tilde{r}(n) &= \ln[r_{\mathcal{R}}(n) + jr_{\mathcal{I}}(n)] = \ln[\rho_r \exp(j\phi_r)] \\ &= \ln[\rho_r] + j\phi_r = \tilde{\rho}_r + j\phi_r, \end{aligned} \quad (16)$$

where  $r_{\mathcal{R}}$  is the signal's real (In-phase) component,  $r_{\mathcal{I}}$  is the imaginary (Quadrature) component,  $\rho_r$  is the magnitude, and  $\phi_r$  is the phase angle [87]. The  $i^{\text{th}}$ , equalized preamble's augmented representation—denoted here in as IQ+NL—is,

$$R^i(m, n) = \begin{bmatrix} r_{\mathcal{R}}^i(1, 1) & r_{\mathcal{R}}^i(1, 2) & \cdots & r_{\mathcal{R}}^i(1, 320) \\ r_{\mathcal{I}}^i(2, 1) & r_{\mathcal{I}}^i(2, 2) & \cdots & r_{\mathcal{I}}^i(2, 320) \\ \tilde{\rho}_r^i(3, 1) & \tilde{\rho}_r^i(3, 2) & \cdots & \tilde{\rho}_r^i(3, 320) \\ \phi_r^i(4, 1) & \phi_r^i(4, 1) & \cdots & \phi_r^i(4, 320) \end{bmatrix}, \quad (17)$$

where  $i = 1, 2, \dots, N_B$  for a total of  $N_B$  preambles,  $m = 1, 2, \dots, N_D$ , and  $n = 1, 2, \dots, 320$  for a IEEE 802.11a Wi-Fi preamble sampled at 20 MHz. Combining the preamble's phase behavior—captured by  $\phi_r$ —with the IQ features provides a computationally efficient mechanism that improves SEI performance under degrading SNR [87]. The rest of this section provides detailed descriptions for the two semi-supervised learning approaches that enable SEI using signal's collected under Rayleigh fading and degrading SNR conditions.

##### A. Multipath Equalization using a Conditional GAN

Prior to RF-DNA fingerprint generation, all signals undergo channel equalization using a Conditional GAN (CGAN), which is introduced by the authors of [105]. The CGAN is constructed using a CAE and CNN for the  $G$  and  $D$ , respectively. The use of semi-supervised training enables estimation of a generative function  $G(z|y)$  capable of reconstructing a Wi-Fi preamble without Rayleigh fading effects despite those effects being present within the preamble input to the  $G$ . Fig. 2 shows the CGAN training and RF signal equalization process developed to generate the results presented in Sect. V. Table II provides the configuration and parameters used to construct the CGAN's  $G$  and  $D$ .

Multipath channel effects are induced by filtering each collected preamble using a unique TDL—given in equation (3)—configured to represent a Rayleigh fading channel consisting of  $L = 5$  reflecting paths. A unique instance of scaled and like-filtered Additive White Gaussian Noise (AWGN) is then added to each preamble to achieve a SNR of 9 dB to 30 dB in 3 dB increments. For each SNR, a total of ten, unique AWGN realizations are generated to augment the data set and facilitate Monte Carlo analysis. The resulting received signal  $r[n]$ —as expressed in equation (4)—is represented using IQ+NL and each feature is re-scaled to be within the range  $[0, 1]$  using Min-Max normalization. The resulting normalized set of  $N_B$  preambles are then randomly assigned to either the training or test set. The training set is comprised of  $N_R = 1800$  (i.e., 90% of the total available at the chosen SNR and noise realization) preambles and the test set consists of  $N_T = 200$  (i.e., 10% of the total available at the chosen SNR and noise realization) preambles where  $N_T = N_B - N_R$ .

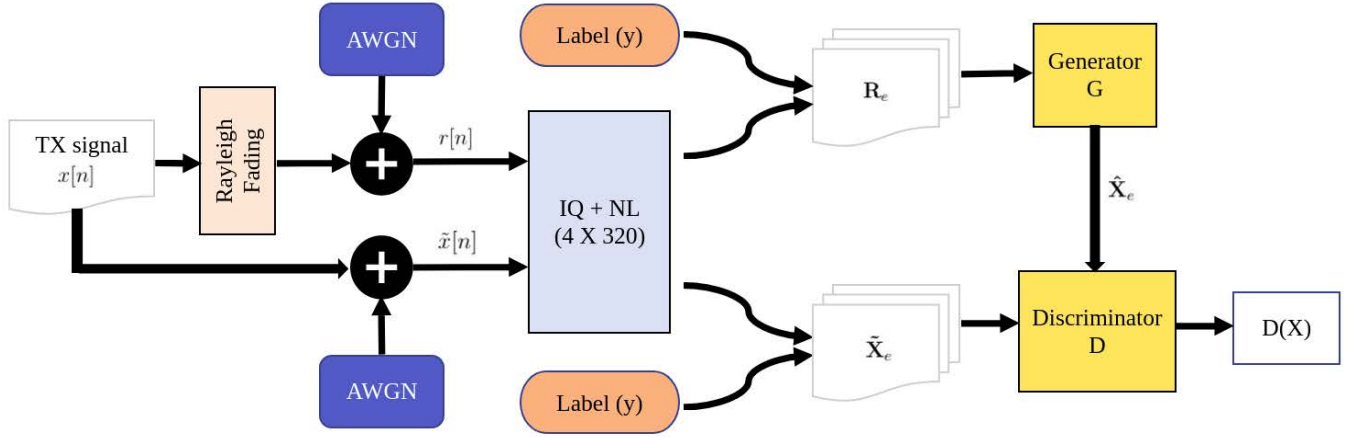


Fig. 2. *CGAN Training*: Flowchart illustrating the process used to train the  $G$  to facilitate channel equalization that preserves the exploited, emitter-specific SEI features.

The CGAN is first proposed in [105] and is an extension of the traditional GAN introduced in [104]. In CGAN, the  $G$  and  $D$  networks—shown in Fig. 2—accept the class label  $y$  as an additional input; thus, both mapping functions  $G(z)$  and  $D(X)$  are conditioned on the variable  $y$  and the traditional GAN’s minimax optimization equation is rewritten as [105],

$$\min_G \max_D V(D, G) = E_{x \sim P_d(x)} \{\log[D(x|y)]\} + E_{z \sim P_z(z)} \{\log[1 - D(G(z|y))]\}, \quad (18)$$

where  $P_d(x)$  is the training data distribution learned by the  $G$ . In this work, the class label is combined with the input to the  $G$  and  $D$  using a hidden representation that enables the GAN to estimate a one-to-many generative function conditioned by  $y$  instead of the traditional one-to-one mapping. The hidden representation is generated by an embedding layer that maps each emitter’s class label to a length fifty vector. It is important to note that the length of the vector is empirically chosen based on [106]. The label vector size is expanded to a length of 1,280 using a dense layer and reshaped into a  $4 \times 320$  tensor to match the dimensionality of its assigned preamble. The  $4 \times 320$  label is appended to the corresponding emitter’s normalized IQ+NL preamble representations to form a  $4 \times 320 \times 2$  labeled preamble representation denoted as  $\mathbf{R}_e$ .

During CGAN training, the  $G$ ’s input is the preamble  $\mathbf{R}_e$  and the  $D$ ’s input is a set of *AWGN-only* preambles  $\tilde{\mathbf{X}}_e$  (i.e., there are no multipath effects present within this signal set). The  $G$  attempts to learn the multipath impacted preambles’ distribution and estimate a function  $G(z)$  that maps them to  $\tilde{\mathbf{X}}_e$  such that the distribution of  $\tilde{\mathbf{X}}_e$  matches the distribution associated with the *AWGN-only* preambles  $\tilde{\mathbf{X}}_e$  used to train the  $D$ . The  $D$  outputs a single-value  $D(x)$  representing the probability that the input  $x$  is from the training data  $\tilde{\mathbf{X}}_e$  rather than  $\tilde{\mathbf{X}}_e$ . The CGAN is trained using backpropagation with a minibatch size of 256 tensors, 10,000 epochs, and an alternating scheme in which the  $D$  is trained for  $S$  steps based upon a given  $G$ . Training for  $S$  steps results in the best version of the  $D$ . The authors of [104] treat  $S$  as a hyperparameter

with  $S = 1$  being the least computationally complex; thus,  $S$  is set to one for the results presented in Sect. V. The  $D$  is trained using forward- and backpropagation with the goal of maximizing  $V(D, G)$  to achieve the highest correct decision probability. After  $S = 1$  steps. The  $G$  is trained using Stochastic Gradient Descent (SGD) to minimize  $V(D, G)$  with the goal of reducing the  $D$ ’s ability to make a correct decision. This training process continues until  $D(x) = 0.5$  everywhere or the total number of training iterations equals the empirically chosen value of 10,000.

TABLE II  
THE CONFIGURATION FOR THE NEURAL NETWORKS ASSOCIATED WITH THE GENERATOR  $G$ , THE DISCRIMINATOR  $D$  AND RF-DNA FINGERPRINT CLASSIFIER USED FOR CGAN EQUALIZED RF-DNA FINGERPRINTING.

Model	Layer	Dimension	Activation
<b>Generator (G)</b>	Input	4 X 320 X 2	none
	Convolution 2D	3 X 3 X 64	relu
	Max Pooling 2D	2 X 2	none
	Convolution 2D	3 X 3 X 32	relu
	Max Pooling 2D	1 X 2	none
	Convolution 2D	2 X 3 X 8	relu
	De-Convolution 2D	2 X 3 X 16	relu
	UP-Sampling	1 X 2	none
	De-Convolution 2D	2 X 3 X 16	relu
	UP-Sampling	2 X 2	none
	De-Convolution 2D	2 X 3 X 8	relu
	Dropout 2D	0.5	none
	De-Convolution 2D	1 X 3 X 2	linear
	<b>Discriminator (D)</b>	Input	4 X 320 X 2
Convolution 2D		3 X 3 X 64	relu
Max Pooling 2D		2 X 2	none
Convolution 2D		3 X 3 X 32	relu
Max Pooling 2D		1 X 2	none
Convolution 2D		3 X 3 X 8	relu
Flatten		none	none
Dropout		0.5	none
Dense		128	relu
Dense		1	sigmoid
<b>Fingerprinting Classifier</b>	Input	4 X 320 X 2	none
	Convolution 2D	3 X 3 X 64	relu
	Max Pooling 2D	2 X 2	none
	Convolution 2D	3 X 3 X 32	relu
	Max Pooling 2D	1 X 2	none
	Convolution 2D	3 X 3 X 8	relu
	Flatten	none	none
	Dropout	0.5	none
	Dense	128	relu
	Dense	4	softmax

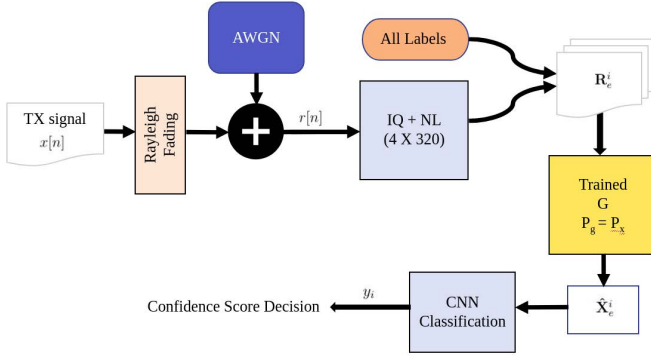


Fig. 3. Illustration of the SEI process that uses a trained CGAN’s  $G$  network to perform multipath channel equalization while simultaneously preserving emitter specific RF-DNA fingerprinting exploited features prior to CNN classification.

Once the CGAN is trained, the resulting  $G$ —that provides the mapping function  $G(z|y, \theta_g)$ —is disconnected from the  $D$  and used to equalize the multipath preambles  $r[n]$  generated from the  $N_T$  preambles comprising the test set of  $x[n]$ . Each test preamble  $r[n]$  is combined with each of the  $N_D = 4$  labels using the hidden representation—described earlier in this section—to create a total of four labeled preambles  $\mathbf{R}_e^i$  where  $i = 1, 2, 3, 4$ . The trained  $G$  generates an equalized output  $\hat{\mathbf{X}}_e^i$  corresponding to each labeled preamble  $\mathbf{R}_e^i$ . Finally, the second channel (a.k.a., the hidden representation label) is removed from the  $G$ ’s outputs  $\hat{\mathbf{X}}_e^i$  prior to classification using a trained CNN. This process is illustrated in Fig. 3.

The CNN is trained using: (i)  $4 \times 320$  formed using the IQ+NL preamble representations generated from the AWGN-only training set  $\tilde{x}[n]$ , (ii) backpropagation, (iii) SGD to minimize the categorical, cross-entropy loss function, (iv)  $l_2$ -norm regularization to reduce overfitting, and (v) Adam optimization for the adjustment of the network’s weights [107]. The CNN’s output layer uses a softmax decision to assign the  $i^{\text{th}}$  equalized representation  $\hat{\mathbf{X}}_e^i$  a label of  $y_i$  according to,

$$y_i = \max_j(Q_{ij}), \quad (19)$$

where  $Q_{ij}$  is the  $j^{\text{th}}$  CNN output for the  $i^{\text{th}}$  equalized representation input  $\hat{\mathbf{X}}_e^i$ ,  $j = [1, 2, 3, 4]$  is the index of the softmax layer outputs, and  $i = [1, 2, 3, 4]$  for a given received preamble  $r[n]$ . Lastly, a confidence score decision is used to assign the received multipath preamble  $r[n]$  a label  $\hat{y}$  that satisfies,

$$\hat{y} = \max_i(y_i) = \max_i \max_j(Q_{ij}). \quad (20)$$

The best possible SEI performance is achieved by training the CNN at SNRs lower than those in the test set. A grid search is performed to determine the best SNR at which to train the CNN and achieve the highest SEI performance across all SNR values. For example, the CNN is trained using preambles collected at an SNR of 12 dB and once trained that CNN classifies preambles collected at each SNR in the range from 9 dB to 30 dB with 3 dB increments between consecutive SNR values. The ‘best’ training SNR is the SNR whose corresponding trained CNN results in the

highest average percent correct classification across all SNR values. The CGAN SEI process can be summarized using the following algorithm,

### B. Multipath Equalization using JCAECNN

This equalization approach uses a joint CAE and CNN (a.k.a., JCAECNN) architecture similar to that used in [61]; however, the approach described here differs from that in [61] in that the CAE architecture is modified to consist of multiple decoder heads instead of one. The decoder heads decompose a received preamble—that undergoes Rayleigh fading—into its  $L$  weighted and delayed copies of the transmitted signal,  $x[n]$ . As illustrated in Fig. 4, the JCAECNN equalization process is built on a Single Input Multiple Output (SIMO) system that includes: signal collection and detection (Sect. III-A), multipath fading and AWGN scaling (Sect. III-C), and signal preparation—in accordance with our prior work [87]—prior to equalization and classification.

Equalization is performed using a CAE consisting of a single encoder and  $L$  decoder heads (i.e., one for each path of the Rayleigh fading channel) using the preambles’ IQ+NL representations at the selected SNR. Motivated by the results presented in [108], a Densely Connected Convolutional Network (DenseNet) is used to implement the “shared” encoder shown in Fig. 4. DenseNet is comprised of multiple Dense blocks where each block is created by connecting each convolutional layer to all preceding convolutional layers of the same size. These dense connections grant each convolutional layer access to all previously generated feature maps to enable feature reuse. In this work, two densely connected blocks are used to construct the encoder. The DenseNet encoder generates compressed representation  $h(\mathbf{R}[m, n])$ , which is the input shared with each of the following NN architectures: the  $L$  decoder heads and the classifier. The resulting JCAECNN architecture is derived from the square error function of equation (8). The optimization goal is to minimize the error between the received signal  $r(m)$  and its delayed and scaled copies  $C_k = \alpha_k x(m - \tau_k)$  generated using the TDL of equation (3). The target of each decoder head is to reconstruct a single copy  $C_k$  corresponding to the  $k^{\text{th}}$  path of the Rayleigh fading channel. In addition to the decoder heads, a CNN classifier (CNN<sub>I</sub>) is used to assign the compressed representation  $h(\mathbf{R}[m, n])$  to any of the  $N_D = 4$  emitters using a softmax decision. The NN configurations for the shared encoder, decoder heads, and CNN<sub>I</sub> classifier are provided in Table III.

The JCAECNN is trained iteratively to jointly optimize the combined loss function given by,

$$F(\theta) = \sum_{k=1}^L [\lambda_k \times M(m, \tau_k) + \lambda_c \times C(y_c, \tilde{y}_c)], \quad (21)$$

where  $\lambda_k$  are the  $k^{\text{th}}$  decoder head’s loss weights corresponding to each Rayleigh fading path,  $\lambda_c$  are CNN’s loss weights,  $M(m, \tau_k)$  is the MSE loss given by,

$$M(m, \tau_k) = \frac{1}{N_s} \sum_{m=1}^{N_s} (x(m - \tau_k) - \hat{x}(m - \tau_k))^2 \quad (22)$$



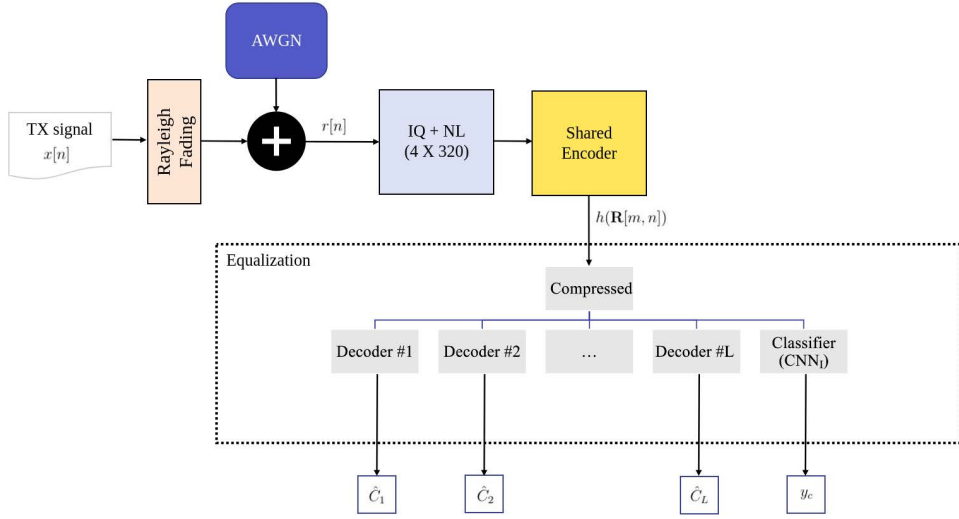


Fig. 4. *JCAECNN Training*: Flowchart illustrating signal pre-processing and the joint CAE multipath equalization.

where  $\hat{x}(m - \tau_k) = \hat{C}_k$  is the decoder's output corresponding to the  $k^{\text{th}}$  path, and  $C(y_c, \hat{y}_c)$  is the categorical cross entropy function used by the CNN classifier to compute the difference between the ground-truth label  $y_c$  and estimated label  $\hat{y}_c$ . If the ground-truth label is one-hot encoded where  $y_c = [y_{c,1}, y_{c,2}, \dots, y_{c,N_D}]$ , the categorical cross entropy can be calculated by the following formula,

$$C(y_c, \hat{y}_c) = - \sum_{l=1}^{N_D} (y_{c,l} \times \log(\hat{y}_{c,l})) \quad (23)$$

where  $l$  is the index of the class at both the one-hot encoded ground truth and the output layer of the classifier [109]. An individual fading path's MSE loss is optimized by updating the weights of the shared encoder and decoder head assigned to the chosen fading path.

Decoder head training allows the shared encoder to learn

compressed and delay-invariant SEI features. The CNN classifier head is trained to minimize the  $C$  loss between the actual label  $y_c$  and the estimated label  $\hat{y}_c$ , which allows the shared encoder to learn more discriminating SEI features than those learned while training the decoder heads.

As shown in Fig. 5, the trained JCAECNN supplies the equalized preambles  $\hat{C}_k$ —for  $k = 1, 2, \dots, L$ —along with the  $\text{CNN}_I$  decision  $\hat{y}_c$  for every normalized IQ+NL preamble representation  $\mathbf{R}[m, n]$  to the discriminating CNN, which is denoted as  $\text{CNN}_D$ .  $\text{CNN}_D$  assigns  $\hat{C}_k$  label  $y_k$  for all  $k$  and decides that the received preamble was transmitted by the emitter whose class label achieves the highest vote out of  $y_k$  and  $y_c$ . The  $\text{CNN}_D$  architecture is similar to the RF-DNA fingerprint classifier architecture shown in Table II and trained using the same data set used to train the JCAECNN with only AWGN present (i.e., there are no multipath effects present within the signal set).

TABLE III

THE CONFIGURATION FOR THE NEURAL NETWORKS ASSOCIATED WITH THE SHARED DENSENET ENCODER, DECODER HEADS, AND RF-DNA FINGERPRINT CLASSIFIER FOR THE JCAECNN RF-DNA FINGERPRINTING

Model	Layer	Dimension	Activation
Shared Encoder (DenseNet)	Input	4 X 320 X 1	none
	Convolution 2D	3 X 3 X 64	relu
	Convolution 2D	3 X 3 X 64	relu
	Convolution 2D	3 X 3 X 64	relu
	Max Pooling 2D	2 X 2	none
	Convolution 2D	2 X 3 X 16	relu
	Convolution 2D	2 X 3 X 16	relu
Decoder Head	De-Convolution 2D	2 X 3 X 16	relu
	UP-Sampling	2 X 2	none
	De-Convolution 2D	3 X 3 X 32	relu
	Dropout 2D	none	none
	De-Convolution 2D	2 X 3 X 8	relu
	De-Convolution 2D	1 X 3 X 1	linear
Fingerprinting Classifier Head	Convolution 2D	2 X 3 X 8	relu
	Max Pooling 2D	1 X 2	none
	Flatten	none	none
	Dropout	0.5	none
	Dense	128	relu
	Dense	4	softmax

## V. RESULTS

This section presents the experimental results and analysis for the RF-DNA fingerprint-based SEI of IEEE 802.11a Wi-Fi emitters whose signals transverse a Rayleigh fading channel and degrading SNR using the CGAN and JCAECNN pro-

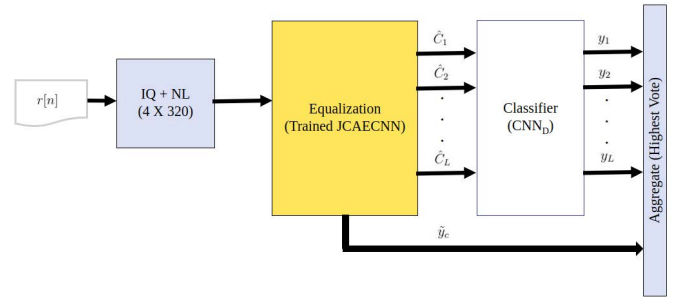


Fig. 5. *JCAECNN Testing*: Flowchart illustrating the RF-DNA fingerprinting process using the trained JCAECNN system that performs channel equalization and supplies the  $\text{CNN}_I$  decision for an aggregated CNN classification decision.

cesses described in Sect. IV-A and Sect. IV-B, respectively. Results for the following experiments are presented.

- 1) *Experiment #1*: Comparative assessment is conducted between the CGAN and JCAECNN approaches and our RF-DNA fingerprinting of emitters under Rayleigh fading published in [38], [41].
- 2) *Experiment #2*: Scalability analysis of the CGAN and JCAECNN approaches. This experiment assesses SEI performance for both approaches using data sets consisting of signals collected from: four, eight, sixteen, and thirty-two commercial emitters to represent larger IoT device deployments.
- 3) *Experiment #3*: Assessment of JCAECNN SEI performance using the sixteen emitter signal set of Experiment #2 as well as the publicly available data sets associated with the published results presented in [88], [89]. This experiment evaluates the JCAECNN architecture’s effectiveness in learning SEI discriminating features from multipath signals whose transmitting emitters differ in manufacturer, model, or Size, Weight, and Power-Cost (SWaP-C) with respect to the emitters described in Sect. III-B. Furthermore, the results of this experiment serve as a benchmark to facilitate the evaluation of future work.
- 4) *Experiment #4*: This experiment assesses JCAECNN SEI performance using a loss function whose weights are selected based upon the Rayleigh fading channel’s path variances. This experiment optimizes the MSE loss weights to maximize JCAECNN performance.

The specifics of the data set(s), training, and testing approaches are explained within each experiment’s section.

#### A. Results for Experiment #1

The IEEE 802.11a Wi-Fi signal set used in this experiment is comprised of preambles extracted from the four Cisco AIR-CB21G-A-K9 Wi-Fi emitters described in Sect. III-B and used to generate the results presented in our prior publications [38], [41]. A total of 2,000 preambles are extracted for each of the four emitters, which is subdivided into a training and testing set comprised of  $N_R = 1,800$  and  $N_T = 200$  randomly selected preambles per emitter. The training set is duplicated to permit creation of a *AWGN-only* set—that is used in the training of the CGAN—and a Rayleigh fading plus AWGN set. The test set is comprised of only Rayleigh fading plus AWGN impacted preambles. It is important to note that the Rayleigh fading channel consists of  $L = 5$  paths, is generated and applied to each signal as described in Sect. III-C, and is unique to each preamble (i.e., the channel coefficients change every transmission). A specific SNR is achieved by adding scaled and like-filtered AWGN to every preamble and the process repeated ten times to permit Monte Carlo simulation. SEI performance is assessed using average percent correct classification performance at SNR values ranging from 9 dB to 30 dB in steps of 3 dB between consecutive values.

Training of the CGAN and JCAECNN approaches is conducted in accordance with Sect. IV-A and Sect. IV-B, respectively. Recall that CGAN SEI performance is maximized by

TABLE IV  
THE TRAINING SNR, DENOED AS  $\text{SNR}_R$ , THAT MAXIMIZES THE CGAN SEI PERFORMANCE WHEN CLASSIFYING TEST SET PREAMBLES AT  $\text{SNR}_T$ . ALL SNR VALUES ARE IN DECIBELS.

$\text{SNR}_T$	$\text{SNR}_R$
9	9
12	9
15	9
18	12
21	15
24	15
27	15
30	18

training it using SNR values lower than those comprising the test set. The results of the grid search—described in Sect. IV-A—are presented in Table. IV in which  $\text{SNR}_R$  designates the SNR of the preambles used to train the CGAN and  $\text{SNR}_T$  is the SNR of the preambles being classified by the CGAN trained at  $\text{SNR}_R$ . The JCAECNN approach’s “best” training SNR is determined using the same approach as that of the CGAN and resulted in a  $\text{SNR}_R$  value of 9 dB for all  $\text{SNR}_T$  values. The Partitioned Time RF Fingerprinting (PTRFF) approach from [41] and traditional Time-Frequency Feature-Engineered RF Fingerprinting (TFRFF) approach from [38] both perform channel correction using the N-M channel estimator and MMSE channel equalizer described in Sect. III-D1 and Sect. III-D2, respectively. The PTRFF approach uses a pre-trained one-dimensional CNN to classify partitioned, time IQ preambles. The time partitions are generated by slicing the IQ samples of each equalized preamble using a  $N_w = 64$  length, sliding window. The TFRFF approach performs feature extraction from the normalized, Gabor coefficients calculated from a preamble’s IQ samples and classification performed using the Multiple Discriminant Analysis/Maximum Likelihood (MDA/ML) classifier. The reader is directed to [41] and [38] for the specific methodologies, results, analysis, and conclusions of the PTRFF and TFRFF approaches, respectively.

Average percent correct classification performance for the CGAN, JCAECNN, PTRFF, and TFRFF SEI approaches are presented in Fig. 6. Each data point is associated with  $N_T \times N_z \times N_D = 8,000$  individual classification decisions. The results of the JCAECNN are generated by setting  $\lambda_k$  and  $\lambda_c$  to one. Compared to the PTRFF, and TFRFF approaches, the results in Fig. 6 show that the CGAN and JCAECNN approaches achieve superior average percent correct classification performance for SNR values of 18 dB and lower. The CGAN approach achieves the best average percent correct classification performance for all SNR values with a maximum of 99.85% at an SNR of 30 dB and a minimum of 95% at an SNR of 9 dB. Based on the results in Fig. 6, DL-based equalization using the semi-supervised learning approaches presented in Sect. IV provides a better mechanism for compensating for multipath channel effects while simultaneously preserving SEI features.

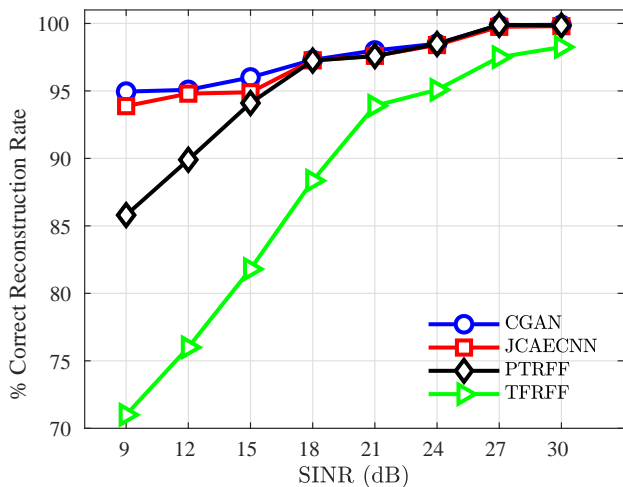


Fig. 6. *Experiment #1 Results:* Average percent correct classification performance across the  $N_D = 4$  IEEE 802.11a Wi-Fi emitters using the CGAN, JCAECNN, PTRFF, and TFRFF approaches for  $\text{SNR} \in [9, 30]$  dB in steps of 3 dB.

### B. Results for Experiment #2

The CGAN and JCAECNN equalization and classification approaches are assessed under an increased number of emitters to reflect larger IoT device deployments. The number of to be identified emitters is:  $N_D = [4, 8, 16, 32]$ . This additional assessment is conducted using the preambles extracted from the signals transmitted by thirty-two TP-Link AC1300 USB Wi-Fi adapters. The assessment is conducted using the following four scenarios.

- *Scenario #1:*  $N_B = 10,000$  preambles extracted from the signals transmitted by Emitter #1 through Emitter #4.
- *Scenario #2:*  $N_B = 10,000$  preambles extracted from the signals transmitted by Emitter #1 through Emitter #8.
- *Scenario #3:*  $N_B = 10,000$  preambles extracted from the signals transmitted by Emitter #1 through Emitter #16.
- *Scenario #4:*  $N_B = 10,000$  preambles extracted from the signals transmitted by Emitter #1 through Emitter #32.

For each scenario, a unique  $L = 5$  Rayleigh fading channel is convolved with each collected preamble prior to adding scaled and like-filtered AWGN to achieve SNR values of 9 dB to 30 dB with 3 dB steps between consecutive SNR values and ten noise realizations per SNR. CGAN and JCAECNN approaches equalize and classify the preambles of each scenario using the same procedure described earlier in this section, but with  $N_R = 8,000$  and  $N_T = 2,000$  for each SNR, noise realization, and emitter. The average percent correct classification of the CGAN and JCAECNN approaches for each of the four scenarios is shown in Fig. 7 where  $\text{CGAN}_i$  and  $\text{JCAECNN}_i$  denote the CGAN and JCAECNN performance results for the  $i^{\text{th}}$  scenario, respectively.

Fig. 7 shows the average percent correct classification results for all four scenarios of Experiment #2. When discriminating four emitters, both approaches result in similar performance as that shown in Fig. 6 with the CGAN approach achieving superior average percent correct classification performance for all SNRs. As the number of to be identified

emitters increases, the performance of the JCAECNN approach begins to surpass that of the CGAN approach. When a total of sixteen emitters are used (a.k.a., Scenario #3), the JCAECNN performance exceeds that of the CGAN approach by a minimum of 1% for all SNRs. When the entire set of thirty-two emitters is used (a.k.a., Scenario #4), the JCAECNN exceeds the performance of the CGAN approach for all SNRs. The smallest improvement is 5% at an SNR of 18 dB and the largest improvement is 11% at an SNR of 9 dB.

Fig. 7 shows that JCAECNN performance suffers less degradation as the number of to be identified emitters increases from four to thirty-two; thus, this approach scales better for larger IoT deployments. The poorer performance of the CGAN approach is attributed to the increasing number of conditional distributions that the  $G$  must learn as the number of emitters goes from four to thirty-two. This is exacerbated by the decreasing efficiency of the hidden label representation. In terms of decision complexity, the JCAECNN performs a total of  $L + 1$  CNN decisions corresponding to the reconstructed  $\hat{C}_k$  and the CNN classifier output  $\hat{y}_c$  for each received preamble  $r[n]$ . The number of JCAECNN classifications does not depend on the number of emitters (i.e., labels), which is not the case for the CGAN. In the CGAN approach, assigning preamble  $r[n]$  to a label  $y$  requires  $N_D$  total equalization actions by the  $G$  that is followed by an additional  $N_D$  sequential classifications. This is due to the fact that the identity of the transmitting emitter is unknown; thus, the preamble must be compared to every known emitter's class. So, as the number of emitters linearly increases so does the number of conditional distributions learned by the  $G$  as well as the number CGAN equalizations and classification decisions.

### C. Results for Experiment #3

Based upon the results presented in Sect. V-B, the results in this section are generated using only the JCAECNN approach. Fig. 8 shows the average percent correct classification per-

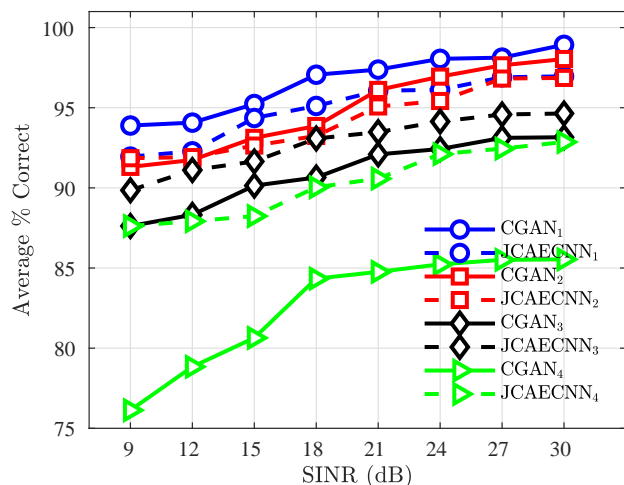


Fig. 7. *Experiment #2 Results:* Average percent correct classification performance across up to  $N_D = 32$  IEEE 802.11a TP-Link adapters using CGAN approach, JCAECNN, for  $\text{SNR} \in [9, 30]$  dB in steps of 3 dB. Note that subscripts denote scenario number.

formance of the JCAECNN approach for the following three different data sets that each contain signals collected from at least sixteen IEEE 802.11a Wi-Fi compliant emitters.

- *Data Set #1*: This data set consists of the IEEE 802.11a Wi-Fi preambles used to generate the Scenario #3 results presented in Fig. 7 and explained in Sect. V-C. This data set’s results are designated using “TP-Link”.
- *Data Set #2*: This data set was collected by the authors of [88] to evaluate the Optimized Radio cAssification through Convolutional neural nEtworks (ORACLE) approach. The data set contains IEEE 802.11a Wi-Fi signals collected from 16 USRP X310 Software-Defined Radios (SDRs) using a stationary Ettus Research USRP B210 SDR as the receiver. It is important to note that the B210 receiver’s sampling rate was set to 5 MHz, which is lower than the 20 MHz sampling rate of the collected signals used to generate the results presented up to this point. This data set’s results are designated using “ORACLE”.
- *Data Set #3*: This data set was collected by the authors of [89] and designated the WiFi Signal (WiSig) data set. The WiSig data set contains IEEE 802.11a Wi-Fi signals captured from a total of 174 transmitting emitters—including USRP B210, X310, and N210 SDRs—over a four day period and using forty-one USRP receivers. In order to maintain consistency with the other two data sets and the rest of this paper’s results only a single day’s and receiver’s worth of WiSig signals are used. The chosen WiSig signals are detected using auto-correlation performed using the preamble’s STS portion and then re-sampled to rate of 20 MHz. This data set’s results are designated using “WiSig”.

Similar to the TP-Link data of Scenario #3, each signal in the Oracle and WiSig data sets is filtered using a unique  $L = 5$  Rayleigh fading channel prior to adding scaled and like-filtered AWGN to achieve SNR values of 9 dB up to 30 dB with 3 dB steps between consecutive SNR values and ten noise realizations per SNR. After that, the JCAECNN approach performs equalization and classification as described earlier in this section. For the sake of consistency, a total of sixteen emitters are randomly selected from the WiSig data set to match the number of emitters represented in the TP-Link and ORACLE data sets. For TP-Link and Oracle data sets,  $N_R = 8,000$  and  $N_T = 2,000$ . For the single day and receiver portion of the WiSig data, the total number of signals collected per emitter is 1,000; thus,  $N_R = 800$  and  $N_T = 200$  to provide a ratio consistent with the other two data sets. The average percent correct classification results presented in Fig. 8 show that JCAECNN equalization and classification of the WiSig preambles achieves superior performance to that of the Oracle data for all SNRs despite the limited number of training samples. That can be attributed to the lower sampling rate used to collect the ORACLE data, which represents only 25% of the sampling rate of the TP-Link and ORACLE data. Additionally, the WiSig data set is comprised of multiple USRP models while the ORACLE signals are transmitted by USRPs that are all the same model. The latter

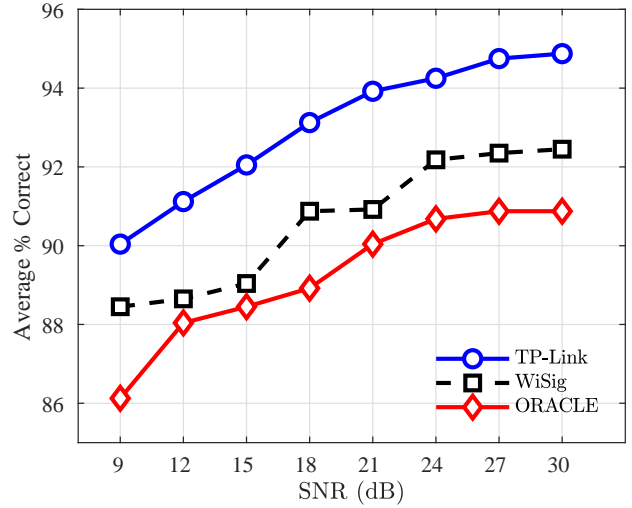


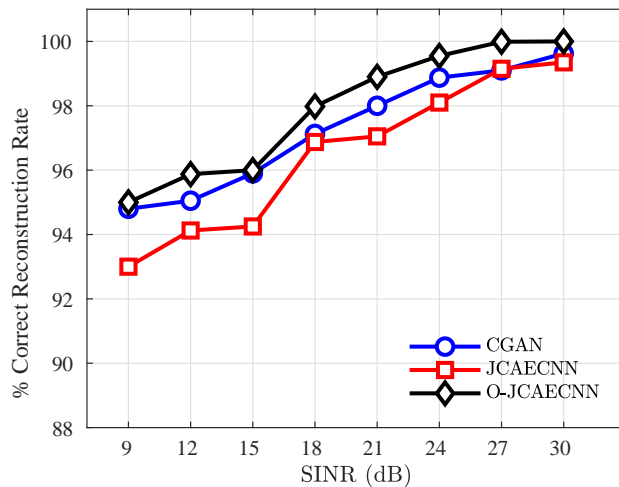
Fig. 8. *Experiment #3 Results*: Average percent correct classification performance for the TP-Link, WiSig, and ORACLE data sets—that each contain signals collected from  $N_D = 16$  IEEE 802.11a Wi-Fi emitters—using the JCAECNN approach for  $\text{SNR} \in [9, 30]$  dB in steps of 3 dB between consecutive values.

is serial number discrimination, which is the most challenging SEI case. Additionally, ORACLE’s USRP X310 is a \$8,500 high-performance SDR made with low variability components, which means less feature variability across SDRs making SEI more difficult [88].

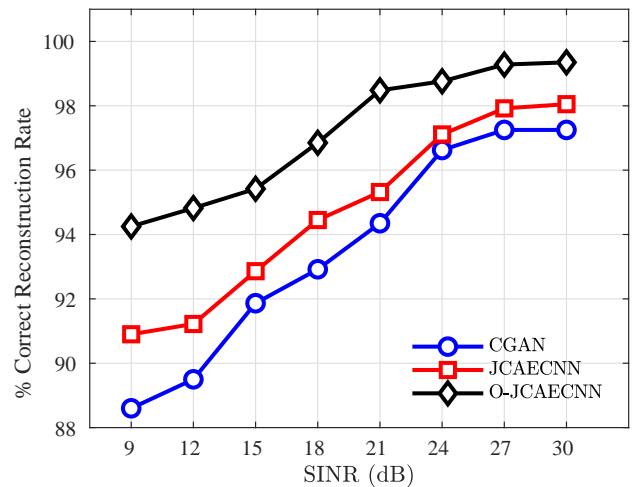
#### D. Results for Experiment #4

Up to this point, all results generated by the JCAECNN approach set  $\lambda_k$  and  $\lambda_c$  to one. In an effort to optimize  $L = 5$  Rayleigh fading channel equalization and classification performance the loss function weights  $\lambda_k$  for  $k = [1, 2, 3, 4, 5]$  and  $\lambda_c$  are set to: thirty-two, sixteen, eight, four, two, and thirty-two, respectively. Selection of these values is based on the fact that the variances of the corresponding Rayleigh channel paths given in equation (2) decay exponentially with  $k$ . Fig. 9 shows the average percent correct classification for the JCAECNN approach with decaying loss weights and is designated as O-JCAECNN in which the ‘O’ denotes ‘optimized’. Comparative assessment is conducted using results generated by: (i) the JCAECNN implementation in which the loss weights are the same (i.e., they are all set to a value of one) and (ii) the CGAN results presented in Fig. 6.

Superior average percent correct classification performance is achieved using the O-JCAECNN approach for all SNR values of 9 dB to 30 dB using a 3 dB step between consecutive values. It is the only SEI approach to achieve an average percent correct classification performance of 100% for  $N_D = 4$  case, which occurs at an SNR of 27 dB and 30 dB. Fig. 10 is the confusion matrix corresponding to the 9 dB O-JCAECNN results presented in Fig. 9(b) and is included to show percent correct classification performance for each of the  $N_D = 16$  emitters. It can be seen that eleven of the sixteen emitters are represented by dark blue diagonal entries, which indicates a percent correct classification performance of at least 95%.



(a)  $N_D = 4$  emitters.



(b)  $N_D = 16$  emitters.

Fig. 9. *Experiment #4 Results*: Average percent correct classification performance across  $N_D$  IEEE 802.11a Wi-Fi TP-Link Adapters using the CGAN, JCAECNN, and O-JCAECNN approaches for SNR $\in$ [9, 30] dB in steps of 3 dB.

The exceptions being Emitter #3, Emitter #4, Emitter #5, Emitter #6, and Emitter #12 of which only Emitter #4 is not classified correctly at least 90% of the time.

The results show that the performance of the JCAECNN model is dominated by: (i) the loss weights in equation (21) that correspond to the first few Rayleigh fading paths, and (ii) the loss weight  $\lambda_c$  corresponding to the CNN<sub>I</sub> classifier head. This suggests that channel-invariant RF-DNA fingerprinting is possible by optimizing the first few and most dominant weights of the JCAECNN’s loss function.

## VI. CONCLUSION AND FUTURE WORK

This work presents and analyzes two semi-supervised DL approaches—designated herein as CGAN and JCAECNN—to enhance IoT security using SEI under Rayleigh fading and degrading SNR. These approaches are capable of extracting discriminating RF-DNA fingerprint features from signals

transmitted by up to thirty-two IEEE 802.11a Wi-Fi emitters while traversing a  $L = 5$  Rayleigh fading channel. The two architectures can reconstruct the transmitted preamble from its received, multipath corrupted version while preserving the SEI discriminating features using the SNR robust, IQ+NL preamble representation. The two semi-supervised learning approaches are compared with the traditional RF-DNA fingerprinting approaches in [38], [41]. The JCAECNN approach shows better scalability as the number of emitters increases from  $N_D = 4$  to  $N_D = 32$ , which is not the case for the CGAN approach due to the number of preamble reconstructions and classification decisions increasing linearly with the number of emitters. The O-JCAECNN results in superior average percent correct classification performance that exceeds 94% for sixteen IEEE 802.11a Wi-Fi emitters at SNR values of 9 dB and higher.

Future research is focused on increasing the viability of SEI-based IoT security by modifying the CGAN and JCAECNN architectures to: (i) allow detection of emitters that are not represented within the training signals set, and (ii) leverage simultaneous training by integrating the collaborative learning scheme presented in [110]. [111] Goldsmith, A. (2005). *Wireless Communications*. Cambridge: Cambridge University Press. doi:10.1017/CBO9780511841224

## REFERENCES

- [1] Maayan, G., “The IoT Rundown For 2020: Stats, Risks, and Solutions,” <https://securitytoday.com/articles/2020/01/13/the-iot-rundown-for-2020.aspx>, Jan. 2020.
- [2] Rawlinson, K., “HP Study Reveals 70 Percent of Internet of Things Devices Vulnerable to Attack,” Jul 2014. [Online]. Available: <https://www8.hp.com/us/en/hp-news/press-release.html?id=1744676>
- [3] Ray, I., D. Kar, J. Peterson, and S. Goeringer, “Device Identity and Trust in IoT-sphere Forsaking Cryptography,” in *International Conference on Collaboration and Internet Computing (CIC)*, 2019.
- [4] Neshenko, N., E. Bou-Harb, J. Crichigno, G. Kaddoum, and N. Ghani, “Demystifying IoT Security: An Exhaustive Survey on IoT Vulnerabilities and a First Empirical Look on Internet-Scale IoT Exploitations,” *IEEE Communications Surveys & Tutorials*, vol. 21, no. 3, pp. 2702–2733, 2019.

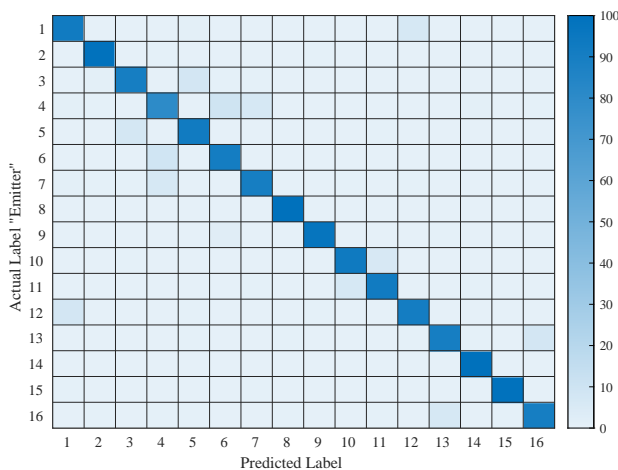


Fig. 10. *Experiment #4 Results*: Confusion matrix showing individual percent correct classification performance for each of the  $N_D = 16$  IEEE 802.11a Wi-Fi TP-Link Adapters provided by Scenario #3 in Sect. V-B using the JCAECNN approach for SNR = 9 dB. Average percent correct classification performance is 94.25%.

- [5] Larsen, S., "A Smart Fish Tank Left a Casino Vulnerable to Hackers," Website: <https://money.cnn.com/2017/07/19/technology/fish-tank-hack-darktrace/index.html>, Jul 2017.
- [6] Wright, J., and J. Cache., *Hacking Wireless Exposed: Wireless Security Secrets and Solutions*, 3rd ed. McGraw-Hill, 2015.
- [7] Stanislav, M., and T. Beardsley, "Hacking IoT: A Case Study on Baby Monitoring Exposures and Vulnerabilities," *Rapid7*, pp. 1–17, 2015.
- [8] Wright, J., "KillerBee: Practical ZigBee Exploitation Framework or 'Wireless Hacking and the Kinetic World,'" pp. 1–39. [Online]. Available: <https://www.inguardians.com/works/>
- [9] Simon, S., "'Internet Of Things' Hacking Attack Led To Widespread Outage Of Popular Websites," *National Public Radio*, Oct 2016. [Online]. Available: <https://www.wbur.org/npr/498954197/internet-outage-update-internet-of-things-hacking-attack-led-to-outage-of-popular>.
- [10] Shipley, P., "Insteon: False Security and Deceptive Documentation," *DEFCON 23*, 2014. [Online]. Available: <https://www.youtube.com/watch?v=dy1LTQLmPtM>
- [11] —. Tools for Insteon RF. 2015. [Online]. Available: <https://github.com/evilpete/insteonrf>
- [12] Brook, C., "Mirai IoT Botnet Co-Authors Plead Guilty," *Digital Guardian*, 2017. [Online]. Available: <https://digitalguardian.com/blog/mirai-iot-botnet-co-authors-plead-guilty/>
- [13] Li, Y., D. Li, W. Cui, and R. Zhang, "Research based on osi model," in *2011 IEEE 3rd International Conference on Communication Software and Networks*, 2011, pp. 554–557.
- [14] Reising, D., "Exploitation of RF-DNA for Device Classification and Verification Using GRLVQI Processing," Ph.D. dissertation, Air Force Institute of Technology, Dec 2012.
- [15] Talbot, C., M. Temple, T. Carbino, and J. Betances, "Detecting Rogue Attacks on Commercial Wireless Insteon Home Automation Systems," *Computers and Security*, vol. 74, pp. 296–307, Oct 2017.
- [16] Sa, K., D. Lang, C. Wang, and Y. Bai, "Specific Emitter Identification Techniques for the Internet of Things," *IEEE Access*, vol. 8, pp. 1644–1652, 2019.
- [17] Reising, D., J. Cancellari, T. D. Loveless, F. Kandah, and A. Skjellum, "Radio Identity Verification-based IoT Security Using RF-DNA Fingerprints and SVM," *IEEE Internet of Things Journal*, vol. 8, no. 10, 2020.
- [18] Pang, J., B. Greenstein, R. Gummadi, S. Seshan and D. Wetherall, "802.11 User Fingerprinting," in *Proceedings of the 13th Annual ACM International Conference on Mobile Computing and Networking*, ser. MobiCom '07. New York, NY, USA: Association for Computing Machinery, 2007, pp. 99–110.
- [19] Dudczyk J., J. Matuszewski and M. Wnuk, "Applying the Radiated Emission to the Specific Emitter Identification," in *International Conference on Microwaves, Radar and Wireless Communications (IEEE Cat. No.04EX824)*, vol. 2, 2004, pp. 431–434.
- [20] Brik, V., S. Banerjee, M. Gruteser, and S. Oh, "Wireless Device Identification with Radiometric Signatures," in *Proceedings of the 14th ACM International Conference on Mobile Computing and Networking*, ser. MobiCom '08. New York, NY, USA: Association for Computing Machinery, 2008, p. 116–127.
- [21] Suski W., M. Temple, M. Mendenhall and R. Mills, "RF Fingerprinting Commercial Communication Devices to Enhance Electronic Security," *International Journal of Electronic Security and Digital Forensics*, vol. 1, no. 3, p. 301–322, Oct 2008.
- [22] Danev B. and S. Kapkun, "Transient-Based Identification of Wireless Sensor Nodes," in *ACM International Conference on Information Processing in Sensor Networks*, Apr 2009, pp. 25–36.
- [23] Klein R., M. Temple, M. Mendenhall and D. Reising, "Sensitivity Analysis of Burst Detection and RF Fingerprinting Classification Performance," in *IEEE International Conference on Communications*, Jun 2009, pp. 1–5.
- [24] Liu, M. and J. Doherty, "Nonlinearity Estimation for Specific Emitter Identification in Multipath Channels," *IEEE Transactions on Information Forensics and Security*, vol. 6, no. 3, pp. 1076–1085, Sep 2011.
- [25] Kennedy, I. and A. Kuzminskiy, "RF Fingerprint Detection in a Wireless Multipath Channel," in *7th International Symposium on Wireless Communication Systems*, Sep 2010, pp. 820–823.
- [26] Williams M., S. Munns, M. Temple and M. Mendenhall, "RF-DNA Fingerprinting for Airport WiMax Communications Security," in *Fourth International Conference on Network and System Security*, Sep 2010, pp. 32–39.
- [27] Takahashi, D., Y. Xiaoa, Y. Zhang, P. Chatzimisios, and H. Chend, "IEEE 802.11 User Fingerprinting and its Applications for Intrusion Detection," *Computers and Math with Applications*, vol. 60, no. 2, pp. 307–318, Jul 2010.
- [28] Tekbas, O., O. Ureten and N. Serinken, "Improvement of Transmitter Identification System for Low SNR Transients," *IEE Electronics Letters*, vol. 40, no. 3, pp. 182–183, 2004.
- [29] Ellis K. and N. Serinken, "Characteristics of Radio Transmitter Fingerprints," *Radio Science*, vol. 36, no. 4, pp. 585–597, 2001.
- [30] Soliman, S. and S-Z. Hsue, "Signal Classification Using Statistical Moments," *IEEE Transactions on Communications*, vol. 40, no. 5, pp. 908–916, 1992.
- [31] Defence R&D Canada - Ottawa, "Interferometric Intrapulse Radar Receiver for Specific Emitter Identification and Direction-Finding," *Fact Sheet REW 224*, Jun 2007.
- [32] Azzouz E. and A. Nandi, *Automatic Modulation Recognition of Communication Signals*. Springer Science & Business Media, 2013.
- [33] Reising D., M. Temple and J. Jackson, "Authorized and Rogue Device Discrimination Using Dimensionally Reduced RF-DNA Fingerprints," *IEEE Transactions on Information Forensics and Security*, vol. 10, no. 6, pp. 1180–1192, 2015.
- [34] Wheeler C. and D. Reising, "Assessment of the Impact of CFO on RF-DNA Fingerprint Classification Performance," in *International Conference on Computing, Networking and Communications*, Jan 2017, pp. 110–114.
- [35] Pan, Y., S. Yang, H. Peng, T. Li and W. Wang, "Specific Emitter Identification Based on Deep Residual Networks," *IEEE Access*, 2019.
- [36] Fadul, M., D. Reising, T. D. Loveless, and A. Ofoli, "Using RF-DNA Fingerprints To Classify OFDM Transmitters Under Rayleigh Fading Conditions," *IEEE Transactions on Information Forensics and Security*, Under Review - Available: <https://arxiv.org/abs/2005.04184> 2020.
- [37] Fadul M., D. Reising, D. Loveless and A. Ofoli, "RF-DNA Fingerprint Classification of OFDM Signals Using a Rayleigh Fading Channel Model," in *IEEE Wireless Communications and Networking Conference (WCNC)*, Apr 2019, pp. 1–7.
- [38] Fadul, M., J. Willis, D. Reising, and T. Loveless, "An Analysis of Process Parameters for the Optimization of Specific Emitter Identification Under Rayleigh Fading," in *Global IoT Summit (GloTS)*, Jun 2022 (Accepted).
- [39] Fadul, M., "The Impact of Rayleigh Fading Channel Effects on the RF-DNA Fingerprinting Process," Master's thesis, University of Tennessee - Chattanooga, Aug 2018.
- [40] Kandah, F., J. Cancellari, D. Reising, A. Altarawneh, and A. Skjellum, "A Hardware-Software Co-design Approach to Identity, Trust, and Resilience for IoT/CPS at Scale," in *International Conference on Internet of Things (iThings) and IEEE Green Computing and Communications (GreenCom) and IEEE Cyber, Physical and Social Computing (CPSCom) and IEEE Smart Data (SmartData)*, July 2019, pp. 1125–1134.
- [41] Fadul, Mohamed K. and Reising, Donald R. and Sartipi, Mina, "Identification of ofdm-based radios under rayleigh fading using rf-dna and deep learning," *IEEE Access*, vol. 9, pp. 17 100–17 113, 2021.
- [42] Defense Advances Research Projects Agency (DARPA), "Spectrum Collaboration Challenge — Using AI to Unlock the True Potential of the RF Spectrum," <https://archive.darpa.mil/sc2/>, 2017.
- [43] Yu, Yiding and Wang, Taotao and Liew, Soung Chang, "Deep-reinforcement learning multiple access for heterogeneous wireless networks," in *2018 IEEE International Conference on Communications (ICC)*, 2018, pp. 1–7.
- [44] O'Shea T. and J. Hoydis, "An Introduction to Deep Learning for the Physical Layer," *IEEE Trans on Cognitive Communications & Networking*, vol. 3, no. 4, Dec 2017.
- [45] Defense Advances Research Projects Agency (DARPA), "Radio Frequency Machine Learning Systems," <https://www.darpa.mil/program/radio-frequency-machine-learning-systems>, 2019.
- [46] Restuccia, F., S. D'Oro, Salvatore, A. Al-Shawabka, M. Belgiovine, L. Angioloni, S. Ioannidis, Stratis and K. Chowdhury, and T. Melodia, "DeepRadioID: Real-Time Channel-Resilient Optimization of Deep Learning-based Radio Fingerprinting Algorithms," in *ACM Int'l Symposium on Mobile Ad Hoc Networking & Computing*, ser. Mobihoc, 2019.
- [47] Restuccia, Francesco and Melodia, Tommaso, "Polymorf: Polymorphic wireless receivers through physical-layer deep learning," in *Proceedings of the Twenty-First International Symposium on Theory, Algorithmic Foundations, and Protocol Design for Mobile Networks*

- and *Mobile Computing*, ser. Mobihoc '20. New York, NY, USA: Association for Computing Machinery, 2020, p. 271–280. [Online]. Available: <https://doi.org/10.1145/3397166.3409132>
- [48] Qin, Zhijin and Ye, Hao and Li, Geoffrey Ye and Juang, Biing-Hwang Fred, “Deep learning in physical layer communications,” *IEEE Wireless Communications*, vol. 26, no. 2, pp. 93–99, 2019.
- [49] Downey, Joe and Hilburn, Ben and O’Shea, Tim and West, Nathan, “In the Future, AIs—Not Humans—Will Design Our Wireless Signals,” *IEEE Spectrum Magazine*, Apr 2020.
- [50] Fadul, Mohamed K. and Reising, Donald R. and Arasu, K. T. and Clark, Michael R., “Adversarial machine learning for enhanced spread spectrum communications,” in *MILCOM 2021 - 2021 IEEE Military Communications Conference (MILCOM)*, 2021, pp. 783–788.
- [51] Baldini, G. and R. Giuliani, “An Assessment of the Impact of Wireless Interferences on IoT Emitter Identification using Time Frequency Representations and CNN,” in *Global IoT Summit (GloTS)*, June 2019, pp. 1–6.
- [52] Baldini, G., C. Gentile, R. Giuliani and G. Steri, “Comparison of Techniques for Radiometric Identification based on Deep Convolutional Neural Networks,” *IET Electronics Letters*, vol. 55, no. 2, pp. 90–92, 2019.
- [53] O’Shea, T., T. Roy, and T. Clancy, “Over-the-Air Deep Learning Based Radio Signal Classification,” *IEEE Journal of Selected Topics in Signal Processing*, vol. 12, no. 1, pp. 168–179, Feb 2018.
- [54] Wong, L., W. Headley, S. Andrews, R. Gerdes and A. Michaels, “Clustering Learned CNN Features from Raw IQ Data for Emitter Identification,” in *IEEE Military Communications Conference (MILCOM)*, Oct 2018, pp. 26–33.
- [55] Mendis, G., J. Wei, and A. Madanayake, “Deep Learning Based Radio-Signal Identification With Hardware Design,” *IEEE Transactions on Aerospace and Electronic Systems*, vol. 55, no. 5, pp. 2516–2531, Oct 2019.
- [56] Riyaz, S., K. Sankhe, S. Ioannidis, and K. Chowdhury, “Deep Learning Convolutional Neural Networks for Radio Identification,” *IEEE Communications Magazine*, vol. 56, no. 9, pp. 146–152, Sep. 2018.
- [57] Merchant, K., S. Revay, G. Stantchev and B. Nossain, “Deep Learning for RF Device Fingerprinting in Cognitive Communication Networks,” *IEEE J. of Selected Topics in Sig Proc*, vol. 12, no. 1, pp. 160–167, Feb 2018.
- [58] Jafari, H., O. Omotere, D. Adesina, H. Wu, and L. Qian, “IoT Devices Fingerprinting Using Deep Learning,” in *IEEE Military Communications Conference (MILCOM)*, Oct 2018, pp. 1–9.
- [59] Guyue, L., Y. Jiabao, Y. Xing, and A. Hu, “Location-Invariant Physical Layer Identification Approach for WiFi Devices,” *IEEE Access*, vol. 7, pp. 06 974–106986, Aug 2019.
- [60] Youssef, K., L. Bouchard, K. Haigh, J. Silovsky, B. Thapa, and C. Valk, “Machine Learning Approach to RF Transmitter Identification,” *IEEE J. of Radio Frequency Identification*, vol. 2, no. 4, pp. 197–205, Dec 2018.
- [61] Yu, J., A. Hu, F. Zhou, Y. Xing, Y. Yu, G. Li, and L. Peng, “Radio frequency fingerprint identification based on denoising autoencoders,” in *2019 International Conference on Wireless and Mobile Computing, Networking and Communications (WiMob)*. IEEE, 2019, pp. 1–6.
- [62] Jian, T., B. Rendon, E. Ojuba, N. Soltani, Z. Wang, K. Sankhe, A. Gritsenko, J. Dy, K. Chowdhury, and S. Ioannidis, “Deep Learning for RF Fingerprinting: A Massive Experimental Study,” *IEEE Internet of Things Magazine*, vol. 3, no. 1, pp. 50–57, 2020.
- [63] Robinson, J., S. Kuzdeba, J. Stankowicz, and J. Carmack, “Dilated Causal Convolutional Model For RF Fingerprinting,” in *2020 10th Annual Computing and Communication Workshop and Conference (CCWC)*, 2020, pp. 0157–0162.
- [64] Ding, Lida and Wang, Shilian and Wang, Fanggang and Zhang, Wei, “Specific emitter identification via convolutional neural networks,” *IEEE Communications Letters*, vol. 22, no. 12, pp. 2591–2594, 2018.
- [65] Chen, Peibo and Guo, Yulan and Li, Gang and Wang, Ling and Wan, Jianwei, “Discriminative adversarial networks for specific emitter identification,” *Electronics Letters*, vol. 56, 02 2020.
- [66] Peng, Linning and Zhang, Junqing and Liu, Ming and Hu, Aiqun, “Deep learning based rf fingerprint identification using differential constellation trace figure,” *IEEE Transactions on Vehicular Technology*, vol. 69, no. 1, pp. 1091–1095, 2020.
- [67] Yang, Ning and Zhang, Bangning and Ding, Guoru and Wei, Yimin and Wei, Guofeng and Wang, Jian and Guo, Daoxing, “Specific emitter identification with limited samples: A model-agnostic meta-learning approach,” *IEEE Communications Letters*, pp. 1–1, 2021.
- [68] Morin, Cyrille and Cardoso, Leonardo S. and Hoydis, Jakob and Gorce, Jean-Marie and Vial, Thibaud’, editor=“Kliks, Adrian and Kryszkiewicz, Paweł and Bader, Faouzi and Triantafyllopoulou, Dionysia and Caicedo, Carlos E. and Sezgin, Aydin and Dimitriou, Nikos and Sybis, Michal, “Transmitter classification with supervised deep learning,” in *Cognitive Radio-Oriented Wireless Networks*. Cham: Springer International Publishing, 2019, pp. 73–86.
- [69] Behura, Sambit and Kedia, Subham and Hiremath, Shrishail M. and Patra, Sarat Kumar, “Wist id—deep learning-based large scale wireless standard technology identification,” *IEEE Transactions on Cognitive Communications and Networking*, vol. 6, no. 4, pp. 1365–1377, 2020.
- [70] McGinthy, Jason M. and Wong, Lauren J. and Michaels, Alan J., “Groundwork for neural network-based specific emitter identification authentication for iot,” *IEEE Internet of Things Journal*, vol. 6, no. 4, pp. 6429–6440, 2019.
- [71] Tang, Peng and Xu, Yitao and Wei, Guofeng and Yang, Yang and Yue, Chao, “Specific emitter identification for iot devices based on deep residual shrinkage networks,” *China Communications*, vol. 18, no. 12, pp. 81–93, 2021.
- [72] Liu, Yongxin and Wang, Jian and Li, Jianqiang and Song, Houbing and Yang, Thomas and Niu, Shuteng and Ming, Zhong, “Zero-bias deep learning for accurate identification of internet-of-things (iot) devices,” *IEEE Internet of Things Journal*, vol. 8, no. 4, pp. 2627–2634, 2021.
- [73] Zha, Xiong and Chen, Huai and Li, Tianyun and Qiu, Zhaoyang and Feng, Yiwei, “Specific emitter identification based on complex fourier neural network,” *IEEE Communications Letters*, pp. 1–1, 2021.
- [74] Gong, Jialiang and Xu, Xiaodong and Qin, Yufeng and Dong, Weijie, “A generative adversarial network based framework for specific emitter characterization and identification,” in *2019 11th International Conference on Wireless Communications and Signal Processing (WCSP)*, 2019, pp. 1–6.
- [75] Ji, Hao and Wan, Tao and Xiong, Wanan and Liao, Jingyi, “A method for specific emitter identification based on surrounding-line bispectrum and convolutional neural network,” in *2020 IEEE 3rd International Conference on Automation, Electronics and Electrical Engineering (AUTEEE)*, 2020, pp. 328–332.
- [76] Gong, Jialiang and Xu, Xiaodong and Lei, Yingke, “Unsupervised specific emitter identification method using radio-frequency fingerprint embedded infogan,” *IEEE Transactions on Information Forensics and Security*, vol. 15, pp. 2898–2913, 2020.
- [77] Li, Rundong and Hu, Jianhao and Li, Shaoqian and Ai, Weiwei, “Specific emitter identification based on multi-domain features learning,” in *2021 IEEE International Conference on Artificial Intelligence and Industrial Design (AIID)*, 2021, pp. 178–183.
- [78] Wang, Yu and Gui, Guan and Gacanin, Haris and Ohtsuki, Tomoaki and Dobre, Octavia A. and Poor, H. Vincent, “An efficient specific emitter identification method based on complex-valued neural networks and network compression,” *IEEE Journal on Selected Areas in Communications*, vol. 39, no. 8, pp. 2305–2317, 2021.
- [79] Qu, Ling-Zhi and Liu, Hui and Huang, Ke-Ju and Yang, Jun-An, “Specific emitter identification based on multi-domain feature fusion and integrated learning,” *Symmetry*, vol. 13, no. 8, 2021. [Online]. Available: <https://www.mdpi.com/2073-8994/13/8/1481>
- [80] Basse, Joshua and Adesina, Damilola and Li, Xiangfang and Qian, Lijun and Aved, Alexander and Kroecker, Timothy, “Intrusion detection for iot devices based on rf fingerprinting using deep learning,” in *2019 Fourth International Conference on Fog and Mobile Edge Computing (FMEC)*, 2019, pp. 98–104.
- [81] Wang, Jian and Zhang, Bangning and Zhang, Jie and Yang, Ning and Wei, Guofeng and Guo, Daoxing, “Specific emitter identification based on deep adversarial domain adaptation,” in *2021 4th International Conference on Information Communication and Signal Processing (ICICSP)*, 2021, pp. 104–109.
- [82] Cun, Chentao and Li, Tianyun and Zhu, Jiawei, “Specific emitter identification based on eye diagram,” in *2021 IEEE 21st International Conference on Communication Technology (ICCT)*, 2021, pp. 1261–1265.
- [83] Peng, Yinan and Zhou, Yuan, “Specific emitter identification via squeeze-and-excitation neural network in frequency domain,” in *2021 40th Chinese Control Conference (CCC)*, 2021, pp. 8310–8314.
- [84] Shen, Weiguo and Wang, Wei, “Node identification in wireless network based on convolutional neural network,” in *2018 14th International Conference on Computational Intelligence and Security (CIS)*, 2018, pp. 238–241.

- [85] Tyler, J., M. Fadul, D. Reising, and F. Kandah, "An analysis of signal energy impacts and threats to deep learning based sei," in *IEEE International Conference on Communications (ICC)*, Jun 2022.
- [86] O'Hara, B. and A. Petrick, *IEEE 802.11 Handbook: A Designer's Companion. Standard Information Network*. IEEE Press, 2005.
- [87] Tyler, J., M. Fadul, D. Reising, and E. Kaplanoglu, "Simplified Denoising for Robust Specific Emitter Identification of Preamble-based Waveforms," in *IEEE GLOBECOM*, Dec 2021.
- [88] Sankhe, Kunal and Belgiovine, Mauro and Zhou, Fan and Riyaz, Shamnaz and Ioannidis, Stratis and Chowdhury, Kaushik, "Oracle: Optimized radio classification through convolutional neural networks," in *IEEE INFOCOM 2019 - IEEE Conference on Computer Communications*, 2019, pp. 370–378.
- [89] Hanna, Samer and Karunartne, Samurdhi and Cabric, Danijela, "Wisig: A large-scale wifi signal dataset for receiver and channel agnostic rf fingerprinting," *IEEE Access*, vol. 10, pp. 22 808–22 818, 2022.
- [90] Lajos, H., A. Yosef, W. Li, and J. Ming, *MIMO-OFDM for LTE, Wi-Fi, and WiMAX*. John Wiley and Sons, Ltd., 2011.
- [91] Liu, M. and J. Doherty, "Specific Emitter Identification using Nonlinear Device Estimation," in *IEEE Sarnoff Symposium*, Mar 2009, pp. 1–5.
- [92] WiSilica, "Top 6 IoT Communication Protocols," <https://wisilica.com/company/top-6-iot-communication-protocols/>, Aug. 2020.
- [93] *IEEE Std 802.11-2007, Local and Metropolitan Area Networks, Part 11: Wireless LAN Medium Access Control (MAC) and Physical Layer (PHY) Specifications*, IEEE, Jun 2007.
- [94] *Agilent E3238 Signal Intercept and Collection Solutions: Family Overview*, Agilent Technology Inc., USA, Publication 5989-1274EN, Jul 2004.
- [95] Hijazi, H. and L. Ros, "Polynomial Estimation of Time-Varying Multipath Gains With Intercarrier Interference Mitigation in OFDM Systems," *IEEE Transactions on Vehicular Technology*, vol. 58, no. 1, Jan 2009.
- [96] Nelder, J. and R. Mead, "A Simplex Method for Function Minimization," *The Computer Journal*, vol. 7, no. 4, pp. 308–313, 1965.
- [97] Lagarias, J., J. Reeds, M. Wright, and P. Wright, "Convergence Properties of the Nelder–Mead Simplex Method in Low Dimensions," *SIAM J. on Optimization*, vol. 9, no. 1, Jan 2006.
- [98] Rugini, L., P. Banelli, and G. Leus, "Simple Equalization of Time-Varying Channels for OFDM," *IEEE Comms Letters*, vol. 9, no. 7, pp. 619–621, Jul. 2005.
- [99] Goodfellow, I., Y. Bengio and A. Courville, *Deep Learning*. MIT Press, 2016, <http://www.deeplearningbook.org>.
- [100] Patterson, J. and A. Gibson, *Deep Learning A Practitioners Approach*. O'Reilly Media, 2017.
- [101] Masci, J., U. Meier, D. Cireşan, and J. Schmidhuber, "Stacked Convolutional Auto-Encoders for Hierarchical Feature Extraction," in *Artificial Neural Networks and Machine Learning – ICANN 2011*, T. Honkela, W. Duch, M. Girolami, and S. Kaski, Eds. Berlin, Heidelberg: Springer Berlin Heidelberg, 2011, pp. 52–59.
- [102] Seyfioğlu, M., A. Özbayoğlu, and S. Gürbüç, "Deep Convolutional Autoencoder for RADAR-based Classification of Similar Aided and Unaided Human Activities," *IEEE Transactions on Aerospace and Electronic Systems*, vol. 54, no. 4, pp. 1709–1723, Aug 2018.
- [103] Creswell, A., T. White, V. Dumoulin, K. Arulkumaran, B. Sengupta, and A. A. Bharath, "Generative adversarial networks: An overview," *IEEE Signal Processing Magazine*, vol. 35, no. 1, pp. 53–65, 2018.
- [104] Goodfellow, Ian and Pouget-Abadie, Jean and Mirza, Mehdi and Xu, Bing and Warde-Farley, David and Ozair, Sherjil and Courville, Aaron and Bengio, Yoshua, "Generative adversarial nets," in *Advances in Neural Information Processing Systems*, vol. 27. Curran Associates, Inc., 2014.
- [105] Mirza, M. and S. Osindero, "Conditional generative adversarial nets," *arXiv*, 2014. [Online]. Available: <https://www.inguardians.com/works/>
- [106] Bogale Gereme, Fantahun and Zhu, William, "Fighting fake news using deep learning: Pre-trained word embeddings and the embedding layer investigated," in *2020 The 3rd International Conference on Computational Intelligence and Intelligent Systems*, ser. CIIS 2020. New York, NY, USA: Association for Computing Machinery, 2020, p. 24–29. [Online]. Available: <https://doi.org/10.1145/3440840.3440847>
- [107] Kigima, D. and J. Ba, "Adam: A method for stochastic optimization," *arXiv*, 2015. [Online]. Available: <https://arxiv.org/pdf/1412.6980.pdf>
- [108] Huang, Gao and Liu, Zhuang and van der Maaten, Laurens and Weinberger, Kilian Q., "Densely connected convolutional networks," in *Proceedings of the IEEE Conference on Computer Vision and Pattern Recognition (CVPR)*, July 2017.
- [109] Polat, Görkem and ergenç, Ilkay and Kani, Haluk and Alahdab, Yesim and Atug, Ozlen and Temizel, Alptekin, "Class distance weighted cross-entropy loss for ulcerative colitis severity estimation," *arXiv preprint arXiv:2202.05167*, 2022.
- [110] Guocong, Song and Wei Chai, "Collaborative learning for deep neural networks," 2018.
- [111] R. S. Sutton and A. G. Barto, *Reinforcement learning: An introduction*. MIT press, 2018.